Transportation Consortium of South-Central States

Solving Emerging Transportation Resiliency, Sustainability, and Economic Challenges through the Use of Innovative Materials and Construction Methods: From Research to Implementation

Alternative Supplementary Cementitious Materials in Ultra-High Performance Concrete

Project No. 21CNMSU60

Lead University: New Mexico State University

Final Report

August 2022

Disclaimer

The contents of this report reflect the views of the authors, who are responsible for the facts and the accuracy of the information presented herein. This document is disseminated in the interest of information exchange. The report is funded, partially or entirely, by a grant from the U.S. Department of Transportation's University Transportation Centers Program. However, the U.S. Government assumes no liability for the contents or use thereof.

Acknowledgments

The authors would like to acknowledge the support and direction of the Project Review Committee that included Dr. Paul Barr of Utah State University, Ken Wylie (Materials Engineer), and Sean Brady of the New Mexico Department of Transportation.

TECHNICAL DOCUMENTATION PAGE

1. **Project No.** 21CNMSU60	**2. Government Accession No.**	**3. Recipient's Catalog No.**

4. Title and Subtitle Alternative Supplementary Cementitious Materials in Ultra-High Performance Concrete	**5. Report Date** August 2022 **6. Performing Organization Code**
7. Author(s) PI: Craig M. Newtson https://orcid.org/0000-0002-2140-9759 GRA: Seyedsaleh Mousavinezhad https://orcid.org/0000-0003-0302-3796 GRA: Gregory J. Gonzales https://orcid.org/0000-0003-4523-9982 GRA: William K. Toledo https://orcid.org/0000-0002-3436-5118 GRA: Judit M. Garcia https://orcid.org/0000-0002-9159-1525	**8. Performing Organization Report No.**
9. Performing Organization Name and Address Transportation Consortium of South-Central States (Tran-SET) University Transportation Center for Region 6 3319 Patrick F. Taylor Hall, Louisiana State University Baton Rouge, LA 70803	**10. Work Unit No. (TRAIS)** **11. Contract or Grant No.** 69A3551747106
12. Sponsoring Agency Name and Address United States of America Department of Transportation Research and Innovative Technology Administration	**13. Type of Report and Period Covered** Final Research Report August 2021 – August 2022 **14. Sponsoring Agency Code**

15. Supplementary Notes
Report uploaded and accessible at: Tran-SET's website (http://transet.lsu.edu/)

16. Abstract
Ultra-high performance concrete (UHPC) is an emerging material with remarkable mechanical and durability properties that contains large amounts of cementitious materials. Silica fume is a main supplementary cementitious material (SCM) in UHPC, however, it is more expensive than cement and other SCMs, so it is often substituted with inexpensive class F fly ash. Unfortunately, future availability of fly ash is uncertain as the energy industry moves toward renewable energy. Fly ash shortages create an urgent need to find cost-effective and environmentally-friendly alternatives for fly ash. This study investigated replacing cement, fly ash, and silica fume in UHPC mixtures with ground granulated blast-furnace slag (GGBFS), metakaolin, and a natural pozzolan (pumicite). To identify acceptable UHPC mixtures (28-day compressive strength greater than 17,000 psi [120 MPa]), workability, compression, and flexural tests were conducted on all mixtures. Then, durability properties including shrinkage, frost resistance, and chloride ion permeability (rapid chloride permeability and surface resistivity tests) were evaluated for the acceptable UHPC mixtures. Results showed that 75, 100, and 40% of the fly ash in the control mixture could be replaced with pumicite, metakaolin, and GGBFS, respectively, while still producing acceptable UHPC mixtures. Flexural strengths were greater than 2000 psi (13.80 MPa) for all mixtures, which should be considered acceptable for many UHPC applications. For durability, the UHPC mixtures had shrinkage strains no greater than 406 μstrain, durability factors of at least 105, and "very low" susceptibility to chloride ion penetration. These results indicate that the durability for all of the UHPC mixtures appears to be excellent. In general, the results indicate that pumicite, metakaolin, and GGBFS are all suitable candidates to replace most or all fly ash and potentially replace some silica fume in UHPC.

17. Key Words Ultra-High Performance Concrete, Flexural Strength, Durability, Supplementary Cementitious Material, Fly Ash, Metakaolin, Natural Pozzolan	**18. Distribution Statement** No restrictions.

19. Security Classif. (of this report)	**20. Security Classif. (of this page)**	**21. No. of Pages**	**22. Price**
Unclassified	Unclassified	45	

SI* (MODERN METRIC) CONVERSION FACTORS

APPROXIMATE CONVERSIONS TO SI UNITS

Symbol	When You Know	Multiply By	To Find	Symbol
		LENGTH		
in	inches	25.4	millimeters	mm
ft	feet	0.305	meters	m
yd	yards	0.914	meters	m
mi	miles	1.61	kilometers	km
		AREA		
in^2	square inches	645.2	square millimeters	mm^2
ft^2	square feet	0.093	square meters	m^2
yd^2	square yard	0.836	square meters	m^2
ac	acres	0.405	hectares	ha
mi^2	square miles	2.59	square kilometers	km^2
		VOLUME		
fl oz	fluid ounces	29.57	milliliters	mL
gal	gallons	3.785	liters	L
ft^3	cubic feet	0.028	cubic meters	m^3
yd^3	cubic yards	0.765	cubic meters	m^3
		NOTE: volumes greater than 1000 L shall be shown in m^3		
		MASS		
oz	ounces	28.35	grams	g
lb	pounds	0.454	kilograms	kg
T	short tons (2000 lb)	0.907	megagrams (or "metric ton")	Mg (or "t")
		TEMPERATURE (exact degrees)		
°F	Fahrenheit	5 (F-32)/9 or (F-32)/1.8	Celsius	°C
		ILLUMINATION		
fc	foot-candles	10.76	lux	lx
fl	foot-Lamberts	3.426	$candela/m^2$	cd/m^2
		FORCE and PRESSURE or STRESS		
lbf	poundforce	4.45	newtons	N
lbf/in^2	poundforce per square inch	6.89	kilopascals	kPa

APPROXIMATE CONVERSIONS FROM SI UNITS

Symbol	When You Know	Multiply By	To Find	Symbol
		LENGTH		
mm	millimeters	0.039	inches	in
m	meters	3.28	feet	ft
m	meters	1.09	yards	yd
km	kilometers	0.621	miles	mi
		AREA		
mm^2	square millimeters	0.0016	square inches	in^2
m^2	square meters	10.764	square feet	ft^2
m^2	square meters	1.195	square yards	yd^2
ha	hectares	2.47	acres	ac
km^2	square kilometers	0.386	square miles	mi^2
		VOLUME		
mL	milliliters	0.034	fluid ounces	fl oz
L	liters	0.264	gallons	gal
m^3	cubic meters	35.314	cubic feet	ft^3
m^3	cubic meters	1.307	cubic yards	yd^3
		MASS		
g	grams	0.035	ounces	oz
kg	kilograms	2.202	pounds	lb
Mg (or "t")	megagrams (or "metric ton")	1.103	short tons (2000 lb)	T
		TEMPERATURE (exact degrees)		
°C	Celsius	1.8C+32	Fahrenheit	°F
		ILLUMINATION		
lx	lux	0.0929	foot-candles	fc
cd/m^2	$candela/m^2$	0.2919	foot-Lamberts	fl
		FORCE and PRESSURE or STRESS		
N	newtons	0.225	poundforce	lbf
kPa	kilopascals	0.145	poundforce per square inch	lbf/in^2

TABLE OF CONTENTS

LIST OF FIGURES

LIST OF TABLES

ACRONYMS, ABBREVIATIONS, AND SYMBOLS

ACRONYMS

AEA	Air-Entraining Admixture
ASR	Alkali-Silica Reaction
ASTM	American Society for Testing Materials
CSH	Calcium Silicate Hydrate
DF	Durability Factor
GGBFS	Ground Granulated Blast-Furnace Slag
HRWRA	High-Range Water-Reducing Admixture
LVDT	Linear Variable Differential Transformers
MOR	Modulus of Rupture
RCPT	Rapid Chloride Permeability Testing
RDM	Relative Dynamic Modulus
SCM	Supplementary cementitious material
Tran-SET	Transportation Consortium of South-Central States

ABBREVIATIONS

Al_2O_3	Aluminum Trioxide
BaO	Barium Oxide
$Ca(OH)_2$	Calcium Hydroxide
CaO	Calcium Oxide
OH^-	Hydroxyl Ions
Fe_2O_3	Iron Oxide
MgO	Magnesium Oxide
MnO_2	Manganese Oxide
P_2O_5	Phosphorus Oxide
K_2O	Potassium Oxide
SiO_2	Silica or Silicon Dioxide
NaCl	Sodium Chloride
NaOJ	Sodium Hydroxide

Na_2O	Sodium Oxide
SrO	Strontium Oxide
SO_3	Sulfur Trioxide
TiO_2	Titanium Dioxide

SYMBOLS

C	a constant that accounts for Poisson's ratio and the specimen's geometry
E_0	the dynamic elastic modulus at zero cycles of freezing and thawing
E_D	dynamic elastic modulus of a specimen
E_n	the dynamic elastic modulus after n cycles
I_0	the current immediately after voltage is applied
I_t	the current at t min after voltage is applied
m	the mass of the specimen
M	the specified number of cycles (300)
N	the number of cycles
n	the measured fundamental frequency
Q_s	the adjusted total charge passed (coulombs) through a3.74-in (95-mm) diameter specimen
Q_x	the total charge passed through a x-in diameter specimen
t	time
x	the diameter of the actual specimen

EXECUTIVE SUMMARY

Ultra-high performance concrete (UHPC) is an emerging cementitious material with remarkable mechanical and durability properties. Exceptional mechanical and durability properties of UHPC include 28-day compression strengths greater than 17,000 psi (120 MPa), high modulus of rupture (MOR) and peak strength (ultimate strength), low susceptibility to shrinkage, and excellent resistance to both frost damage and chloride ion penetration. These exceptional properties of UHPC can be attributed to: 1) its high cementitious materials content that includes supplementary cementitious materials (SCMs) such as silica fume and class F fly ash, 2) its very low water to cementitious materials ratio (w/cm), and 3) its high density. Dense microstructure of UHPC is achieved through careful selection of constituent materials to ensure an optimized gradation and maximized particle-packing density as well as detailed preparation methods to properly mix and cure UHPC.

While silica fume is a very reactive SCM that also improves particle-packing density, it is substantially more expensive than other SCMs because it needs to be shipped long distances for use in North America. In the last two decades, inexpensive class F fly ash has been used in UHPC to replace silica fume and produce sustainable UHPC. Unfortunately, class F fly ash is becoming difficult to procure and its future availability is uncertain because of changes in the energy industry. Coal-fired power plants have been taken offline or been refitted to gas-fired plants as the energy industry has invested in renewable energy production. The cost of silica fume and the lack of availability of fly ash are driving the need for cost effective and environmentally-friendly alternatives for silica fume and fly ash. Potential SCMs that may be suitable substitutes for fly ash and silica fume in UHPC mixtures include natural pozzolan (pumicite), metakaolin, and ground granulated blast-furnace slag (GGBFS).

This study is aimed at investigating non-proprietary UHPC mixtures produced by replacing a broad range of portland cement, fly ash, and silica fume with three sustainable SCMs. The three SCMs used in this study included locally available natural pozzolan, metakaolin, and a GGBFS obtained from Michigan, USA. Slump and slump flow tests were conducted for all mixtures to identify mixtures with acceptable workability. Mechanical properties of acceptable mixtures were then evaluated using compression and flexural tests to identify mixtures that met the minimum 28-day compressive strength requirement of 17,000 psi (120 MPa) for UHPC. It should be noted that cube specimens (instead of cylindrical specimens) were used for compression tests because cubes do not require end preparation (grinding). After identification of acceptable UHPC mixtures, shrinkage was evaluated for up to 56 days (28 days moist curing and 28 days air curing) by monitoring length changes of UHPC specimens. Frost resistance of the UHPC mixtures was also assessed for UHPC specimens exposed to 300 cycles of freezing and thawing. Finally, chloride ion permeability of UHPC mixtures was investigated by conducting rapid chloride permeability tests (RCPTs) and surface resistivity tests on 56-day UHPC specimens.

Workability tests results were consistent enough to achieve acceptable slump and slump flow values for individual mixtures in no more than two attempts and only 27 trials were produced to identify 16 acceptable mixtures in terms of workability.

Compressive strength tests conducted on the 16 mixtures were then used to identify 13 mixtures that met the minimum 28-day compressive strength (17,000 psi [120 MPa]) requirement for UHPC. The three mixtures that did not qualify as UHPC were mixtures that replaced 100% of fly

ash with pumicite, used metakaolin to replace 25% of silica fume and 100% of fly ash, and replaced 10% portland cement, 100% of fly ash, and 10% of silica fume with GGBFS and metakaolin. Although these three mixtures did not meet the 28-day compressive strength requirement, they were able to achieve 56-day compressive strengths that exceeded 20,020 psi (138 MPa), which should be suitable for many UHPC applications. This observation indicates that a more liberal definition of UHPC could capture the longer-term benefits provided by SCMs such as pumicite, metakaolin, or GGBFS.

Results from compression tests indicate that replacing fly ash or silica fume with any of the SCMs used in this study decreased the seven-, 28-, and 56-day compressive strengths, regardless of the amount of replacement. However, all mixtures had 56-day compressive strengths greater than 20,000 psi (137.9 MPa) indicating that long-term benefits of these mixtures are probably worth evaluating. Additionally, reductions in 56-day compressive strengths caused by replacing fly ash (but not silica fume) with alternative SCMs were of less magnitude than reductions at seven and 28 days. The fact that the pumicite, metakaolin, and GGBFS mixtures had comparable 56-day compressive strengths to that of the control mixture, after having lower seven- and 28-day strengths than the control mixture, indicates that the reactions of the alternative SCMs had finally progressed to the point that they were essentially equivalent to the fly ash reaction at 56 days.

Flexural tests showed that all mixtures using pumicite, metakaolin, or GGBFS to replace fly ash (but not silica fume) had first peak (modulus of rupture [MOR]) and peak strength (ultimate strength) values greater than 2685 psi (18.50 MPa) and 2800 psi (19.30 MPa), respectively, which were comparable to those for the control mixture. The greatest MOR (2995 psi [20.65 MPa]) and peak strength (3230 psi [22.25 MPa]) were obtained when 100% of the fly ash was replaced with 50% pumicite and 50% metakaolin. The residual strengths (f_{600} and f_{150}) presented similar trends to those for MOR and peak strength. The flexural tests also revealed that mixtures that replaced silica fume with alternative SCMs (after replacing 100% of the fly ash) had a significant reduction in MOR and peak strength. However, these values were still greater than 2000 psi (13.80 MPa) and may be considered acceptable UHPC flexural strengths. Note that these relatively large reductions in MOR and peak strength should be considered when attempting to replace silica fume in UHPC mixture proportions.

Total shrinkage values at 56 days for all of the UHPC mixtures were less than 406 μstrain, which is below the 500 μstrain maximum limit used by many state departments of transportation. It was observed that shrinkage decreased as pumicite or metakaolin content increased or GGBFS content decreased. It was also observed that replacing 40% of the fly ash with GGBFS produced the greatest shrinkage while replacing 100% of the fly ash with 50% pumicite and 50% metakaolin produced the least shrinkage. This can be attributed to GGBFS being more angular and slightly larger than the spherical fly ash particles, which can lead to less refinement of the capillary pores. However, since pumicite and metakaolin particles are much smaller than fly ash particles, a combination of the two can cause greater refinement of the capillary pores that reduces drying shrinkage by obstructing evaporation of capillary water. Another mechanism to reduce shrinkage is the slow reactivity of the pumicite that can delay shrinkage until the skeletal structure has formed and helps restrain shrinkage.

Freezing and thawing tests showed that all UHPC mixtures had durability factor (DF) values between 105 and 109, indicating that UHPC mixtures were extremely resistant to degradation caused by freezing and thawing cycles, regardless of SCM type. The results also showed that

relative dynamic modulus (RDM) values for all UHPC mixtures were comparable and replacing fly ash or silica fume with any of the alternative SCMs used in this study, or a combination of these SCMs, did not significantly change the RDM and DF values. The results also showed that RDM values increased slightly during the freezing and thawing cycles which can be attributed to specimens containing un-hydrated cementitious materials that were able to react throughout the duration of the test causing an increase in dynamic modulus. These results show that pumicite, metakaolin, and GGBFS all appear to be suitable replacements for fly ash and silica fume in terms of frost resistance

The 56-day RCPT results showed that all UHPC mixtures produced in this study were categorized as having "very low" chloride ion penetration (total charge passed of between 109 and 165 coulombs). Replacing fly ash with any of the alternative SCMs in this study decreased total charge passed (chloride ion permeability). However, replacing silica fume with pumicite or metakaolin increased chloride ion penetration, most likely due to the pumicite and metakaolin particles being larger than silica fume particles and producing less refined capillary pores.

Surface resistivity tests were performed at 56 days to be consistent with 56-day RCPTs. The surface resistivity values for all UHPC mixtures ranged between 15.2 kΩ-in (386 kΩ-mm) and 23.7 kΩ-in (603 kΩ-mm), indicating that the chloride ion penetration for all of the UHPC mixtures was "very low." Similar to the RCPT results, replacing fly ash with any of the alternative SCMs improved chloride ion permeability (increased surface resistivity) and the greatest improvement in chloride ion permeability occurred when all of the fly ash was replaced with metakaolin (surface resistivity value of 23.7 kΩ-in [603 kΩ-mm]). However, replacing silica fume with pumicite or metakaolin increased chloride ion penetration, which is also consistent with the RCPT results. Increasing chloride ion penetration with decreasing silica fume content is again attributed to the larger pumicite and metakaolin particles (than silica fume) producing less refined capillary pores.

It is concluded that natural pozzolan (pumicite), metakaolin, and GGBFS can be promising alternatives for fly ash and silica fume in UHPC mixtures. Pumicite was able to replace up to 75% of the fly ash and metakaolin was able to replace up to 100% of the fly ash and 25% of the silica fume while producing 28-day compressive strengths greater than 17,000 psi (120 MPa). Additionally, replacing fly ash and silica fume with alternative SCMs, regardless of the SCM type and amount, produced low susceptibility to shrinkage and excellent resistance to both frost damage and chloride ion penetration.

1. INTRODUCTION

Ultra-high performance concrete (UHPC) is an emerging type of concrete material with exceptional mechanical and durability properties. According to ASTM C1856 (1), UHPC must have a minimum 28-day compressive strength of 17,000 psi (120 MPa). To reach to this strength, UHPC requires high contents of cementitious materials because it contains no coarse aggregates and has a very low water to cementitious materials ratio (w/cm). Additionally, high contents of supplementary cementitious materials (SCMs) including silica fume and class F fly ash (10-30% of the cementitious materials mass) are used in UHPC to improve density, mechanical, and durability properties. However, silica fume is expensive compared to other cementitious materials because it needs to be shipped long distances for use in North America (2). Additionally, the future availability of class F fly ash in North America is uncertain because of changes in the energy industry. Coal-fired power plants have been taken offline or been refitted to gas-fired plants as the energy industry has invested in renewable energy production. The cost of silica fume and the lack of availability of fly ash are driving the need for cost effective and environmentally-friendly alternatives for silica fume and fly ash. Potential SCMs that may be suitable substitutes for fly ash and silica fume in UHPC mixtures include natural pozzolan (pumicite), metakaolin, and ground granulated blast-furnace slag (GGBFS).

This research aimed to investigate the possibility of using three SCMs including a natural pozzolan, metakaolin, and GGBFS as potential alternatives for portland cement, fly ash, and silica fume to be included in non-propriety UHPC proportions. First of all, the effects of replacing portland cement, fly ash, and silica fume with a natural pozzolan, metakaolin, and GGBFS on workability, compressive and flexural strengths of sixteen mixtures were assessed to identify acceptable UHPC mixtures. After identifying acceptable UHPC mixtures, durability characteristics including shrinkage, frost resistance, and chloride ion permeability (rapid chloride permeability and surface resistivity tests) were investigated.

2. OBJECTIVES

The overall objective of this study was to assess the ability of a natural pozzolan (pumicite), metakaolin, and GGBFS to replace portland cement, fly ash, and silica fume in UHPC mixtures. The evaluation was initiated by testing workability, compressive, and flexural strength of mixtures containing a broad range of pumicite, metakaolin, GGBFS, and combinations of these SCMs to identify acceptable UHPC mixtures.

Once cementitious materials combinations were identified that would provide acceptable UHPC properties, the next objective was to assess how pumicite, metakaolin, and GGBFS affected mechanical and durability properties of UHPC. UHPC mixtures were developed with a broad range of pumicite, metakaolin, GGBFS, fly ash, and silica fume contents. The UHPC mixtures were evaluated for strength and durability properties. Durability related tests that were conducted included shrinkage, frost resistance, rapid chloride permeability, and surface resistivity tests.

3. LITERATURE REVIEW

This chapter provides a literature review for UHPC, SCMs such as fly ash, silica fume, natural pozzolans, metakaolin, and GGBFS that may affect UHPC performance, and durability issues such as shrinkage, freezing and thawing, and corrosion of reinforcing steel as well as a review of UHPC durability testing methods. Durability properties addressed in this work include shrinkage and frost resistance that may indicate susceptibility to cracking that would facilitate ingress of moisture and harmful chemical compounds as well as rapid chloride permeability and surface resistivity that are indicators of corrosion susceptibility for reinforcing steel.

3.1. Ultra-High Performance Concrete

UHPC, a modern type of cementitious materials with exceptional mechanical and durability properties, became commercially available in the US in 2000 (3). That version of UHPC consisted of portland cement, ground quartz, fine sand, silica fume, an accelerating admixture, a high-range water reducing admixture (HRWRA), and 2% by volume of steel fibers (4). According to ASTM C1856 (1), UHPC must have a 28-day compressive strength greater than 17,000 psi (120 MPa). To identify suitable UHPC mixtures, many researchers have investigated various UHPC mixture proportions, the effects of using various fibers in UHPC, and rheological properties of fresh UHPC (*5, 6*). Transportation agencies have reported compressive strengths greater than 21,700 psi (150 MPa) and sustained post-cracking tensile strengths greater than 720 psi (5 MPa) for some UHPC products (3).

3.1.1. Properties of Ultra-High Performance Concrete

UHPC's unique properties provide the potential to significantly increase the service life and durability of new and existing concrete structures. UHPC properties are achieved through careful selection of its constituent materials to ensure optimized gradation and maximized packing density, as well as detailed preparation methods to properly mix and cure UHPC (7).

UHPC's exceptional mechanical properties include 28-day compressive strength greater than 17,000 psi (120 MPa), high flexural strength, high ductility when fiber reinforced, and substantial energy absorption (*1, 8, 9*). More importantly, UHPC has excellent durability properties such as low porosity, high microstructure density, a discontinuous pore structure that reduces liquid ingress, resistance to chemical and physical attacks, low chloride ion permeability, resistance to frost damage, negligible alkali-silica reaction (ASR), and excellent abrasion resistance (*6, 8–12*). In cases where UHPC is used as a repair material, it has been shown to exhibit excellent adhesive strength for a broad range of surface roughness (4).

It should be noted that long-term properties of UHPC may be influenced by casting procedures since the dispersion and orientation of the fiber reinforcement is greatly influenced by placement methods. Some placement methods cause the fibers to show a preference for aligning in the direction of flow during casting. The ability of the fibers to remain in suspension is dependent on the rheology of the concrete. Consequently, an optimized gradation of granular materials should be targeted (3).

3.1.2. Development of Ultra-High Performance Concrete

In the 1990s, Richard and Cheyrezy (9) used ultra-fine and highly reactive components with thermal treatment to develop reactive powder concretes (RPC) with excellent workability. RPC is a major milestone in the development of UHPC. RPC mixtures evolved into what is now UHPC

that use high contents of cementitious materials, very low w/cm, silica fume, fine quartz powder, quartz sand, HRWRA and steel fibers (*9, 13, 14*). Coarse aggregates were eliminated to increase homogeneity. The compressive strength of RPC ranged from 29,000 psi (200 MPa) to 116,000 psi (800 MPa) (9). In the late 1990s, the first UHPC developed through RPC technology was commercialized under the name Ductal® (*15, 16*).

UHPC development has progressed rapidly since 2000, leading to sustainable, inexpensive non-proprietary UHPC with remarkable mechanical and durability properties. Despite successful implementation of proprietary UHPC in new structures, widespread adoption has been slow due to the high cost of the materials and production (17). Use of local materials in non-proprietary UHPC mixtures provides an opportunity to produce economical and sustainable alternatives to proprietary products. Previous UHPC research at New Mexico State University has shown that UHPC produced with locally available materials and SCMs, such as silica fume and class F fly ash, exhibit comparable mechanical and durability properties to proprietary UHPC mixtures (*7, 10, 18*). Incorporation of locally available materials can reduce materials cost up to 70% compared to proprietary UHPC (*19, 20*). Researchers have also investigated the possibility of using different SCMs in UHPC to replace portland cement and sustainably reduce portland cement consumption as well as to replace SCMs that are either costly or difficult to obtain (*21, 22*).

3.1.3. Applications of Ultra-High Performance Concrete

For the past two decades, UHPC has garnered interest in many countries with a broad range of applications including building components, bridges, architectural features, repair and rehabilitation, vertical components such as windmills towers and utilities towers, oil and gas industry applications, off-shore structures, and hydraulic structures. Among these applications, road and bridge construction have been the most popular. Using UHPC for bridges and bridge components has been implemented in Australia, Austria, Canada, China, the Czech Republic, France, Germany, Italy, Japan, Malaysia, the Netherlands, New Zealand, Slovenia, South Korea, Switzerland, and the United States (*15, 23*).

In 1997, the first RPC structure in the world was constructed, a pedestrian bridge in Sherbrooke, Canada (*24, 25*). Elsewhere, Malaysia started studying UHPC in 2006 and built its first UHPC bridge in 2010. To date, more than 100 UHPC bridges have been constructed in Malaysia (*23, 26*). In France, many bridges, facades, and slabs have been constructed with UHPC (26). In Switzerland, UHPC has been mostly used for in-situ repair or strengthening of existing structures (27). UHPC bridges have also been built in the Netherlands and Spain (*28–30*).

In the United States, UHPC has seen growing applications in repair and construction of highway infrastructure to extend service life (31). UHPC has been used in simple-span pre-stressed concrete girder bridges where the tensile strength was utilized to allow elimination of mild steel shear reinforcement. UHPC has also been used in a deck bulb-double-tee girders to produce desirable rheological behavior and accelerate construction (3). The Mars Hill Bridge in Wapello Country, Iowa was the first UHPC road bridge constructed in the US in 2006 (32) and the first US usage of UHPC as a bridge deck overlay was completed in 2016 on a reinforced concrete slab bridge located in Brandon, Iowa (33).

Over the past few years in the United States, the Federal Highway Administration (FHWA) has adopted UHPC as a grouting material for connections between bridge components (4). In 2009, UHPC was used to create deck-level connections between precast concrete elements for a bridge

in the state of New York. In one case, UHPC was used in transverse connections between precast deck panels. In another case, it was used in longitudinal connections between the top flanges of deck bulb-tee girders (3).

UHPC has also been investigated for other applications such as precast concrete piles, seismic retrofit of bridge substructures, thin bonded overlays, and security and blast mitigation applications (34).

3.2. Supplementary Cementitious Materials in UHPC

Although ASR is unlikely to occur in UHPC, SCMs have been used in UHPC to mitigate other durability problems such as chloride penetration, freezing and thawing, and sulfate attack. In many cases, the SCMs have also been shown to improve mechanical properties of UHPC. Silica fume and fly ash are two of the most commonly used SCMs in UHPC. Other SCMs, such as natural pozzolans, metakaolin, and GGBFS have also been used to improve mechanical and durability properties of UHPC.

3.2.1. Silica Fume

Silica fume is a byproduct obtained from the production of silicon alloys. Silica fume consists primarily of fine (less than 0.00004 in. [1 μm]) silica (SiO_2) particles and is highly pozzolanic (35). The silica fume fills voids in the next larger granular class (cement) and produces secondary calcium silicate hydrate (CSH) through pozzolanic reactions (*9, 36*). The fineness of silica fume particles can cause an increase in water demand and require additional admixtures to maintain workability without increasing the w/cm. Because of its fine particles, silica fume can increase the density of concrete as well as greatly improve strength and impermeability of concrete (37). Unfortunately, silica fume is substantially more expensive than other SCMs in North America (2).

3.2.2. Fly Ash

Fly ash is the most commonly used SCM in concrete and has been used since the 1930s. It is a byproduct of coal combustion produced from power plants. There are two classifications of fly ash, Class F and Class C fly ash, that are generally composed of varying amounts of calcium oxide (CaO), Na_2O, K_2O, magnesium oxide (MgO), sulfur trioxide (SO_3), SiO_2, aluminum trioxide (Al_2O_3), and iron oxide (Fe_2O_3) (*37, 38*). The chemical composition determines the ability of a fly ash to improve durability of UHPC. According to ASTM C 618 (1), class C and class F fly ashes contain a minimum of 50 and 70% for the combination of SiO_2, Al_2O_3, and Fe_2O_3, respectively. It has been shown that UHPCs with comparable durability properties and strength greater than 21,800 psi (150 MPa) can be produced with up to 70% replacement of cement with class F fly ash, without employing any special curing or fibers (39).

3.2.3. Pumicite and Other Natural Pozzolans

Natural pozzolans are raw or calcined natural materials with pozzolanic properties. Pozzolans are a diverse class of siliceous or siliceous and aluminous materials that possess little or no cementitious ability when used alone, but are capable of producing cementitious properties when reacting with calcium hydroxide in the presence of water at normal temperatures that can greatly improve concrete durability and performance (*40–43*). Pumicite is amorphous and produced by the release of gases during the solidification of lava. Its cellular structure contains bubbles or air voids that result from gases being trapped in the molten lava during rapid cooling. Although these voids are elongated and parallel to one another, they are sometimes interconnected (44).

Using natural pozzolan as a SCM can reduce the heat of hydration and improves durability properties including resistance to sulfate attack and ASR (45). Ahmad et al. (46) showed that partially replacing cement and silica fume with a natural pozzolan did not substantially affect workability and mechanical properties of UHPC mixtures, however, it did result in very low to negligible chloride ion permeability and less than 500 μstrain drying shrinkage.

Sarıdemir (47), reported that 25% pumicite addition to high strength concrete reduced 28-day compressive strength and modulus of elasticity. Other research has shown that 10% pumicite contributed significantly to microstructural density in high strength concrete, improved 180-day compressive and indirect tensile strengths, improved resistance to chloride ion penetration, and reduced 90-day water absorption (48). Research has also shown that addition of pumicite powder to concrete reduces slump. Kabay et al. (49) observed that replacement of cement with pumicite powder, fly ash, and blends of pumicite and fly ash produced concrete with lower water absorption, sorptivity, void content, and lower early-age compressive and splitting tensile strengths.

Adding more, or coarser, pumicite to concrete may also reduce compressive strength and heat of hydration while increasing water demand and setting time as well as improving sulfate and ASR durability characteristics (*50*, *51*). Liu et al. (52) reported that using pumicite without stimulating additives, such as sodium silicate and potassium fluoride, had low pozzolanic activity. In other research, mixtures containing fly ash, pumicite, or both had less 91-day compressive strength but more rapid strength development beyond 28 days than ordinary concrete (53). Additionally, self-compacting concrete produced with pumicite demonstrated good workability and achieved greater compressive strength at 120 days compared to mixtures without pumicite (54). Pumicite has also been shown to produce acceptable resistance to freezing and thawing when used to replace up to 20% of the cement in concrete mixtures. However, 30% Pumicite decreased frost resistance significantly, as measured by durability factor (DF) (55).

3.2.4. Metakaolin

Metakaolin is an inexpensive SCM produced by calcination of kaolin. Metakaolin consists of silica and alumina that react with calcium hydroxide at room temperature and form CSH gel which increases the density of concrete and reduces porosity. Since metakaolin is manufactured, its production can be tightly controlled to produce a consistent, highly reactive SCM.

It has been found that using metakaolin with cement and fly ash in UHPC can lead to less drying shrinkage compared to when cement and silica fume are used in UHPC (56). Metakaolin and silica fume have been found to be similar in terms of strength development and durability, showing that metakaolin has the potential to replace silica fume (57). Compressive and flexural strengths of UHPC did not substantially change when all of the silica fume (25% of the cement) was replaced with metakaolin (58). However, increases in compressive and flexural strengths were observed when replacing 10-15% of cement with metakaolin (59).

Tafraoui et al. (60) reported that inclusion of metakaolin in UHPC mixtures to replace silica fume resulted in acceptable durability properties. It has been also found that using metakaolin decreases chloride permeability of UHPC (61). Rangaraju and Li (62) reported that workability, time of set, and drying shrinkage decreased with increasing metakaolin content in UHPC. Additionally, using metakaolin in UHPC reduced the diffusion coefficient due to its high specific surface area and extremely fine particles (63). Ternary UHPC mixtures containing metakaolin, fly ash, and cement have been shown to have comparable performance with those containing only silica fume (62).

3.2.5. GGBFS

GGBFS, a by-product of extracting iron from iron ore in a blast-furnace, has been used for many years in concrete production. GGBFS is highly cementitious and is known as a suitable alternative for cement, fly ash, and silica fume in UHPC to improve durability properties (64). Slag is typically composed of CaO, SiO_2, Al_2O_3, and MgO, along with some other oxides in small quantities. It has a glassy structure and produces CSH as a hydration product (37). When portland cement is hydrated it produces CSH and calcium hydroxide ($Ca(OH)_2$), the $Ca(OH)_2$ reacts with the GGBFS and causes a chemical reaction that breaks down the chemical composition of the GGBFS and separates it into a calcium rich phase and a silica rich phase. The phases then react with water to form CSH. A 50% cement replacement minimum is usually needed to effectively mitigate durability issues such as ASR (37) in normal concrete. A higher cement replacement is needed, compared to fly ash, due to its chemical composition and specific chemical reactions. GGBFS is a slow reacting SCM that can require additional curing time and lead to scaling susceptibility.

Researchers have suggested that up to 35% of the cement can be replaced with GGBFS without significantly decreasing compressive strength (*64, 65*). Additionally, it has been found that using GGBFS in combination with silica fume improves flowability (66). GGBFS is generally expected to increase autogenous shrinkage (67). Researchers have also shown that replacing 50% of the cement with GGBFS can produce 28-day compressive strengths comparable to an UHPC control mixture (greater than 21,800 psi [150 MPa]) although it can increase drying shrinkage in the first 24 hours, long-term autogenous shrinkage, and flowability (*68–70*). Additionally, replacing 100% of the silica fume (by volume) with GGBFS in UHPC has been shown to decrease autogenous shrinkage without significantly changing the compressive strength (71).

3.3. Durability Issues

3.3.1. Shrinkage

Shrinkage is the contraction of concrete volume due to the hydration reaction (chemical shrinkage), moisture loss to evaporation and hydration (drying shrinkage and self-desiccation), and decreasing temperature (thermal shrinkage). In this work, shrinkage is considered to occur in two stages: early-age shrinkage that occurs within the first 24 hours and long-term shrinkage that occurs after an age of 24 hours.

Early-age shrinkage consists of three phases: the liquid, skeletal structure, and hardening phases (72). The liquid phase commences as soon as the cementitious materials come into contact with water. During this phase, the concrete has no solid structure and cannot sustain stresses. Consequently, shrinkage in the liquid phase will only cause particles to shift and allow excess water to migrate to the surface. The second phase begins when cement hydration starts to form a skeletal structure (approximately initial set). The hardening phase occurs when the skeletal structure can sustain stresses. Long-term shrinkage can occur for several years and is dependent on several factors such as the chemical composition of the cementitious materials, amount of water in the original concrete mixture, surrounding environment, moisture conditions, and the size of the specimen.

SCMs have been shown to decrease shrinkage by modifying the microstructure of the cement paste. Specifically, SCMs can help densify the concrete and create smaller pores in the matrix to reduce shrinkage (73). Research has shown that the ability of SCMs to reduce shrinkage is determined by the chemical composition of the SCM and the size and distribution of pores (73).

In the case of fly ash, research has shown that increasing cement replacement by fly ash decreases both drying and autogenous shrinkage (74).

Shrinkage can be assessed by measuring the change in size of a specimen. Typically, a specimen's length is monitored throughout its curing period and changes in length, relative to the initial length, quantify the amount of shrinkage that has occurred.

3.3.2. Freezing and Thawing

A cycle of freezing and thawing can cause degradation when the pore spaces in the concrete are filled (or nearly so) with water that will expand as it approaches its freezing temperature. When water freezes, it expands approximately 9%. As soon as the water expands, it causes internal pressure in the concrete. If the internal pressure exceeds the tensile strength of the concrete, it can cause the pore space to dilate and rupture (75). Microcracking near a pore can eventually lead to macrocracking, scaling, and severe degradation of the concrete after numerous cycles of freezing and thawing.

Research has shown that freezing and thawing effects can be mitigated by incorporating entrained air in the concrete. Air-entraining admixtures (AEAs) are usually used to improve frost resistance by creating air bubbles, ranging from 0.0004 to 0.04 in. (10 to 1000 μm) in diameter, in the cement paste that create space that can facilitate the expansion of ice in the concrete to prevent cracking (*35, 76*). Side effects that often occur when using AEAs include decreased strength and stiffness of the concrete (76). SCMs with high or variable carbon contents can jeopardize a concrete mixture's ability to entrain air and also make the air void system inconsistent across multiple batches of concrete (77).

Damage caused by freezing and thawing can be assessed by exciting vibration in specimens over a broad range of frequencies and recording the frequency with the greatest amplitude of acceleration. The frequency recorded is the resonant frequency for first mode vibration (fundamental frequency) and is related to the elastic modulus and density of the specimen (72). The fundamental frequency is used to determine the relative dynamic modulus (RDM), which can be monitored over multiple cycles of freezing and thawing to obtain an indication of the level of deterioration in a specimen.

3.3.3. Corrosion of Reinforcing Steel

Corrosion of reinforcing steel is the leading cause of deterioration in concrete structures. Corrosion is often initiated when harmful ions, such as chlorides, penetrate concrete and reach the reinforcing steel. Chloride ion penetration can occur through capillary absorption, hydrostatic pressure, diffusion, or evaporative transport (78). Corrosion of the steel creates ferrous oxide (rust) that occupies greater volume than the reactants. This expansion exerts internal tensile stresses in the concrete that can cause cracking in the surrounding concrete that can extend to the surface of the concrete and allow even more chloride ions to penetrate the concrete and accelerate the corrosion process. To protect reinforcing steel from corrosion, it is essential to limit chloride ion penetration into the concrete.

One way to improve resistance to chloride ion penetration is to use SCMs or other mineral admixtures to improve density by partially filling pore spaces. The SCMs produce secondary CSH that fills pore spaces to decrease pore volume and increase density. The pore volume in the cement paste largely controls the permeability of concrete and is affected by the cementitious materials

used in the mixture and construction practices (79). High contents of SCMs and steel fibers used in UHPC lead to a dense microstructure which improves resistance to corrosion (12).

3.4. Durability Testing

3.4.1. Shrinkage Testing

ASTM C157 (80) presents the most commonly used method to measure shrinkage strain in concrete specimens. The method specifies monitoring length changes using a length comparator. First, specimens are cured for 23.5 ± 0.5 hours before they are removed from the molds for recording an initial reading using the length comparator. Then, specimens are wet cured for 28 days at 73 ± 3°F (23 ± 2°C). After 28 days wet curing, the second reading is recorded and specimens are stored for an additional period of up to 64 weeks in an environment with, preferably, a relative humidity of 50 ± 4 % and a temperature of 73 ± 3°F (23 ± 2°C). During drying, specimens should be stored with a clearance of at least 1 in (25 mm) on all sides. Finally, average length changes for a period of up to 64 weeks are used to compute shrinkage strain.

3.4.2. Freezing and Thawing Testing

To assess frost resistance of UHPC mixtures according to ASTM C666, Procedure A (81), mass and fundamental transverse frequency of prism specimens exposed to freezing and thawing cycles are measured at intervals no greater than 36 cycles to compute RDM.

Specimens should be cured in the moist room to an age of 13 days. Immediately after the curing period, the temperature of specimens should be decreased to 40°F (4°C) in a water bath in the 24 hours prior to initiating freezing and thawing cycles. For Procedure A, specimens in the freezing and thawing chamber should be completely surrounded by not less than 1⁄32 in (1 mm) nor more than 1⁄8 in (3 mm) of water at all times. A full cycle of freezing and thawing consists of rapidly decreasing the temperature from 40 to 0°F (4 to -18°C) and increasing the temperature from 0 to 40°F (-18 to 4°C) in not less than two nor more than five hours. For Procedure A, not less than 25% of the time should be used for thawing. The period of transition between the freezing and thawing phases of the cycle should not exceed 10 mins, except when specimens are being tested.

On the thawed portion of the cycle, at intervals no greater than 36 cycles, specimens should be removed from the freezing and thawing chamber to determine the mass and fundamental frequency of each specimen. Finally, tested specimens should be returned to the chamber at 40°F (4°C). Each specimen should be tested until it is subjected to 300 cycles or until its RDM decreases to 60 % of the initial modulus, whichever occurs first.

The impact resonance method (ASTM C215 [82]) is used to measure fundamental frequency at various ages by striking a supported specimen with an instrumented hammer and recording the acceleration response history using a lightweight accelerometer attached to the specimen as shown in Figure 1. Fundamental frequency, resonant frequency for first mode vibration, is determined by identifying the frequency at which the maximum acceleration response occurs from a plot of amplitude versus frequency as shown in Figure 2.

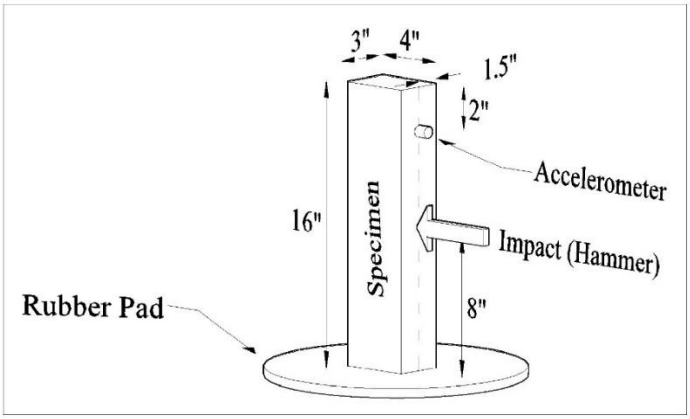

Figure 1. Schematic of fundamental transverse frequency test.

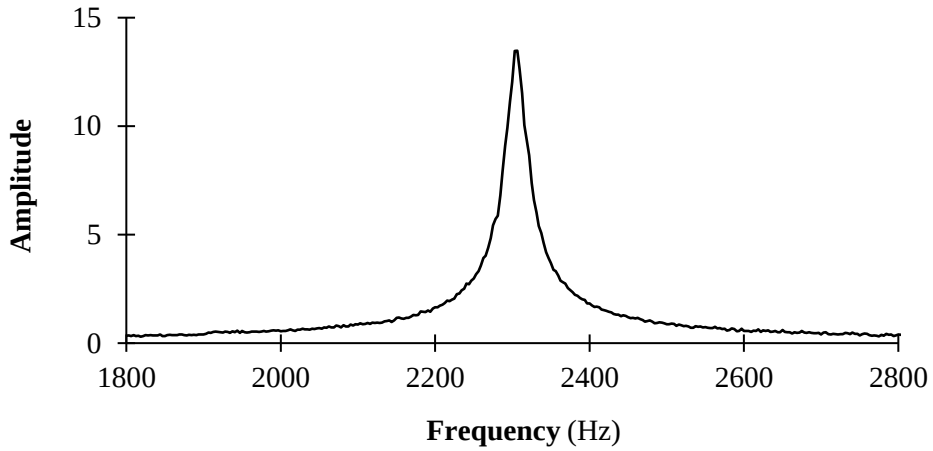

Figure 2. Amplitude versus frequency graph.

At intervals no greater than 36 cycles, fundamental transverse frequency and mass are used to calculate dynamic elastic modulus (E_D) according to ASTM C215 (82):

$$E_D = C \times m \times n^2 \qquad [1]$$

where C is a constant 0.0733 s^2/in^2 (1114 m^{-1}) determined from the geometry of the specimen and an assumed Poisson's ratio (0.167), m is mass (lb [kg]), and n is fundamental transverse frequency (Hz). Then, RDM is computed as:

$$RDM = \frac{E_n}{E_0} \times (100) \qquad [2]$$

where E_n and E_0 are dynamic elastic modulus (psi [Pa]) values after n and 0 cycles, respectively.

3.4.3. Chloride Ion Permeability Testing

Chloride ion permeability can be assessed by conducting RCPT or surface resistivity testing that determine electrical conductance and resistivity of the concrete mixture, respectively. Results from these tests provide indications of the ability of the concrete to resist penetration of chloride ions.

3.4.3.1. Rapid Chloride Permeability Testing

To assess the durability of mixtures against chloride ion penetration, a RCPT is commonly conducted according to ASTM C1202 (83). A 2-in (51-mm) slice cut from a 4 by 8 in (102 by 203 mm) cylinder specimen is placed in a vacuum desiccator and the internal pressure is rapidly decreased to less than 0.96 psi (6650 Pa). The slice is subjected to the vacuum pressure for three hours before being submerged in deionized water for one hour with the vacuum pump running. The specimen is kept in the vacuum desiccator for an additional 18 hours while the pump is off. Then, the specimen is placed in a testing cell with one side of the specimen exposed to a 3.0% sodium chloride (NaCl) solution and the other side of the specimen exposed to a 0.3 N sodium hydroxide (NaOH) solution. This test is performed using a power supply that is set to 60V DC and current is measured every 30 minutes for six hours. Negative and positive terminals of the power supply are connected to the 3.0% NaCl solution and 0.3 N NaOH solution, respectively. The total charge passed (coulombs), a measure of the electrical conductance of the concrete during the period of the test, is calculated as:

$$Q_x = 900 \times (I_0 + 2I_{30} + 2I_{60} + \cdots + 2I_{300} + 2I_{330} + I_{360}) \qquad [3]$$

$$Q_s = Q_x \times (\frac{95}{x})^2 \qquad [4]$$

where Q_x is the total charge passed (coulombs) through a x-in diameter specimen, Q_s is the adjusted total charge passed (coulombs) through a 3.74-in (95-mm) diameter specimen, x is the diameter of the actual specimen (in [mm]), I_0 is the current (amperes) immediately after voltage is applied, and I_t is the current (amperes) at t min after voltage is applied.

In this test, greater electrical conductance indicates that the specimen is more permeable. The interpretation of RCPT results, according to ASTM C1202 (83), is presented in Table 1.

Table 1. RCPT interpretation.

Chloride Ion Penetrability	**RCPT (total charge passed)** (coulombs)
High	>4000
Moderate	2000-4000
Low	1000-2000
Very Low	100-1000
Negligible	<100

3.4.3.2. Surface Resistivity Testing

The surface resistivity test is another common test to provide a rapid indication of chloride ion permeability for concrete mixtures. AASHTO T 358 (84) describes the surface resistivity test, where an alternating current (AC) potential difference is applied by the outer pins (current electrodes) of a four-pin Wenner probe array that generates current flow in the concrete, and the resultant potential difference between the two inner pins (potential electrodes) is measured (Figure 3). The current used and resultant potential, along with the affected specimen area, are used to calculate the surface resistivity of the concrete. It should be noted that the cylindrical specimen used in this test should be wet throughout testing.

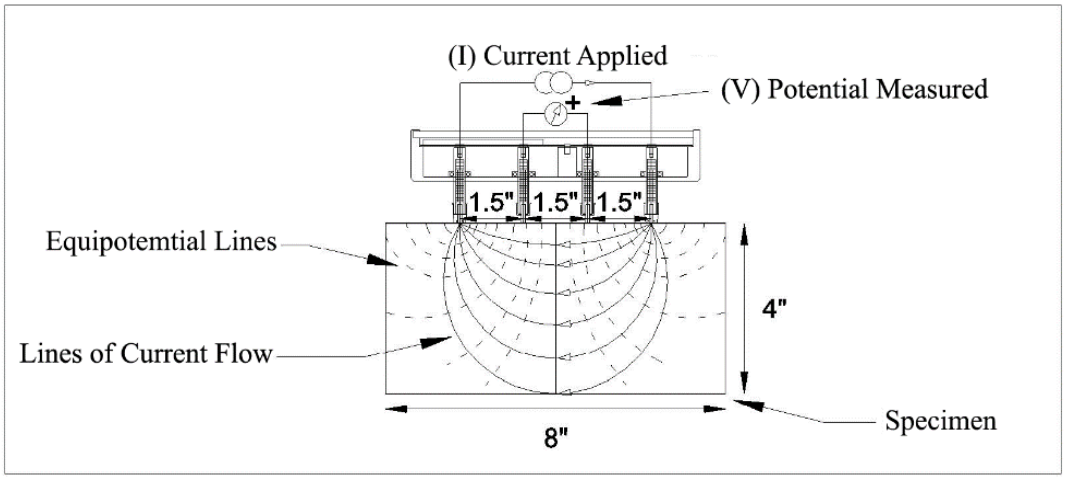

Figure 3. Four-point Wenner probe array test setup.

Surface resistivity (kΩ-in [kΩ-mm]), a measure of the electrical resistivity of the concrete during the test, is related to the resistance of the concrete to chloride ion penetration. According to AASHTO T 358 (84), less electrical resistivity in the specimen indicates that the specimen is more permeable (Table 2).

Table 2. Surface resistivity test interpretation.

Chloride Ion Penetrability	**Surface Resistivity Test** kΩ–in (kΩ-mm)
High	<4.7 (120)
Moderate	4.7-8.3 (120-210)
Low	8.3-14.6 (210-370)
Very Low	14.6-100 (370-2540)
Negligible	>100 (2540)

4. METHODOLOGY

The following sections describe the materials used in this study as well as the methods used for mixing, workability measurements, compression and flexural tests, shrinkage testing, frost resistance testing, RCPT, and surface resistivity testing.

4.1. Materials

4.1.1. Aggregates and Cementitious Materials

Table 3 presents the physical properties and particle size distribution of the local sand (the only aggregate used in this study) obtained from Las Cruces, New Mexico, USA. The cementitious materials used in this study included a Type I/II low-alkali portland cement produced by GCC, a class F fly ash produced at the San Juan generating station in northern New Mexico, a commercially available silica fume (MasterLife SF 100), a natural pozzolan (pumicite) mined near Espanola, New Mexico, a metakaolin (GMK-S5) manufactured by Grace in Aiken, South Carolina, and a GGBFS obtained from St. Marys Cement in Detroit, Michigan. Table 4 presents chemical and physical properties of the cementitious materials used in this study.

Table 3. Physical properties and particle size distribution (percent passing) of sand.

Bulk Specific Gravity	**Fineness Modulus**	**Moisture Content** (%)	**Absorption** (%)	**Sieve No.**					
				4	**8**	**16**	**30**	**50**	**100**
2.51	2.81	0.7	1.6	100	93.2	81.5	62.1	45.6	11.7

Table 4. Chemical and physical properties of cementitious materials (%mass).

Chemical Properties	**Material**					
	Cement Type I/II	**Class F Fly Ash**	**Silica Fume**	**Pumicite**	**Metakaolin**	**GGBFS**
CaO	63.9	8.99	0.3	0.40	0.87	38.44
SiO_2	20.3	53.16	96.9	76.29	63.86	42.87
Al_2O_3	4.6	24.64	0.2	12.13	31.11	11.61
Fe_2O_3	3.4	4.22	0.2	1.74	1.06	0.92
MgO	1.91	1.25	0.2	0.07	0.18	4.29
Na_2O	0.23	1.66	0.2	4.23	1.08	0.96
K_2O	0.38	1.24	0.3	4.29	0.09	0.12
TiO_2	-	-	-	0.10	-	-
MnO_2	-	-	-	0.08	-	-
P_2O_5	-	-	-	0.02	-	-
SrO	-	-	-	0.01	-	-
BaO	-	-	-	0.01	-	-
SO_3	2.86	0.25	0.1	0.00	0.05	0.17
Loss on Ignition	2.24	-	2.17	-	1.18	1.96
Physical Properties						
Specific Gravity	3.15	1.91	2.20	2.45	2.60	2.91
Spec. Surface Area (m^2/kg)	335	734	26810	17348	22320	542
Autoclave Expansion (%)	0.05	0.01	-	-	-	0.06

4.1.2. Other Materials

Steel fibers used in this study were NYCON-SF type 1 with 0.5 in (13 mm) length, 0.008 in (0.2 mm) diameter, and tensile strength of 285,000 psi (1900 MPa). To achieve the acceptable workability, a commercially available polycarboxylate-based HRWRA produced by BASF Construction Chemicals (MasterGlenium 3030 NS) was also used.

4.2. Mixture Proportions

An existing UHPC mixture (S10-F10) with 20% SCM (by mass of cementitious materials), w/cm of 0.14, and 1.5% steel fibers (by volume) used in previous research associated with the New Mexico Department of Transportation was selected as a control mixture (85). Table 5 presents proportions for all sixteen mixtures produced in this study. For each mixture, the target slump values were between 4 in (100 mm) and 8 in (205 mm) and acceptable slump flow values were between 8 in (205 mm) and 16 in (405 mm). To interpret the names of the mixtures, the letters denote the type of the SCM used in the mixture (S for silica fume, F for fly ash, N for natural pozzolan, M for metakaolin, and G for GGBFS), and the number after each letter denotes the percent of that SCM in the cementitious materials (by mass). For example, S10-N2-M6-G2 indicates a mixture with SCM composed of 10% silica fume, 2% natural pozzolan (pumicite), 6% metakaolin, and 2% GGBFS as percentages of the total cementitious materials.

Table 5. Concrete mixture proportions.

Mixture Name	Cement lb/yd^3 (kg/m^3)	Silica Fume lb/yd^3 (kg/m^3)	Fly Ash lb/yd^3 (kg/m^3)	Pumicite lb/yd^3 (kg/m^3)	Metakaolin lb/yd^3 (kg/m^3)	GGBFS lb/yd^3 (kg/m^3)	Sand lb/yd^3 (kg/m^3)	Water lb/yd^3 (kg/m^3)	Fiber lb/yd^3 (kg/m^3)	HRWRA gal/yd^3 (ml/m^3)
S10-F10 (Control Mixture)	1413 (839)	176 (104)	176 (104)	0	0	0	1548 (919)	247 (147)	200 (119)	11.41 (56,500)
S10-F5-N5	1413 (839)	176 (104)	88 (52)	88 (52)	0	0	1558 (925)	247 (147)	200 (119)	11.98 (59,330)
S10-F2.5-N7.5	1413 (839)	176 (104)	44 (26)	132 (78)	0	0	1570 (931)	247 (147)	200 (119)	11.98 (59,330)
S10-N10	1413 (839)	176 (104)	0	176 (104)	0	0	1569 (931)	247 (147)	200 (119)	12.55 (62,150)
S10-F5-M5	1413 (839)	176 (104)	88 (52)	0	88 (52)	0	1539 (913)	247 (147)	200 (119)	13.12 (64,980)
S10-F2.5-M7.5	1413 (839)	176 (104)	44 (26)	0	132 (78)	0	1553 (921)	247 (147)	200 (119)	13.12 (64,980)
S10-M10	1413 (839)	176 (104)	0	0	176 (104)	0	1554 (922)	247 (147)	200 (119)	13.69 (67,800)
S10-F8-G2	1413 (839)	176 (104)	141 (83)	0	0	35 (21)	1551 (920)	247 (147)	200 (119)	11.98 (59,330)
S10-F6-G4	1413 (839)	176 (104)	106 (62)	0	0	70 (42)	1553 (921)	247 (147)	200 (119)	12.55 (62,150)
S10-N5-M5	1413 (839)	176 (104)	0	88 (52)	88 (52)	0	1561 (926)	247 (147)	200 (119)	13.12 (64,980)
S10-N2-M6-G2	1413 (839)	176 (104)	0	35 (21)	106 (62)	35 (21)	1555 (923)	247 (147)	200 (119)	13.69 (67,800)
S9-M9-G2	1413 (839)	159 (94)	0	0	159 (94)	35 (21)	1561 (926)	247 (147)	200 (119)	13.69 (67,800)
S9-M9-G12*	1272 (755)	159 (94)	0	0	159 (94)	177 (105)	1563 (928)	247 (147)	200 (119)	13.12 (64,980)
S7.5-N2.5-M10	1413 (839)	132 (78)	0	44 (26)	176 (104)	0	1584 (940)	247 (147)	200 (119)	12.55 (62,150)
S7.5-M12.5	1413 (839)	132 (78)	0	0	220 (130)	0	1574 (934)	247 (147)	200 (119)	13.12 (64,980)
S5-M15	1413 (839)	88 (52)	0	0	264 (156)	0	1595 (946)	247 (147)	200 (119)	12.55 (62,150)

*In this mixture, an additional 10% of cement was replaced with GGBFS.

4.3. Mixing

Mixing was performed in a 4.25 ft^3 (0.12 m^3) capacity pan mixer as shown in Figure 4. The mixing sequence began with sand and cementitious materials for each mixture being placed in a pan mixer prior to starting the mixer. After starting the mixer, water and HRWRA were added with the mixer running and the top of the mixer covered to prevent evaporation. After 15 mins of mixing or when the mixture appeared to be uniformly mixed, whichever was longer, steel fibers were added and the mixer was run for an additional five mins before discharging the mixture. Immediately after mixing, slump and slump flow tests were conducted for each batch.

Figure 4. Concrete mixer.

For each mixture, a 2.0 ft^3 (0.057 m^3) batch was used to produce nine 3.94 in (100 mm) cube specimens, five 4 by 8 in (102 by 203 mm) cylinder specimens, and eight 3×4×16 in (76×102×406 mm) prism specimens, three of which had gauge studs (contact points) embedded in each end of the prism specimen. All specimens were de-molded 24 ± 4 hours after placement and moist cured at 98% relative humidity and a temperature of 73 ± 3°F (23 ± 2°C) for up to 56 days according to ASTM C511 (86). Three cubes for compression testing were cured for seven days, three prisms for frost resistance testing were cured for 14 days, three cubes and five prisms for compression, flexural, and shrinkage testing were cured for 28 days, and three cubes and five cylinders for compression testing, RCPT, and surface resistivity testing were cured for 56 days.

4.4. Slump Test

One of the workability tests performed in this study was the slump test described in ASTM C143 (87). A steel slump cone that had a height of 12 in. (305 mm), a base diameter of 8 in. (203 mm), and a top diameter of 4 in. (102 mm) was used to perform the slump tests. The cone was placed on an even surface and filled in three equal (volumetrically) lifts with each lift rodded 25 times. The concrete was then struck off at the top of the cone to remove any excess concrete. The steel cone was then removed in a single motion by lifting it in the vertical direction. After inverting the steel cone and placing it next to the slumped concrete, the slump was immediately measured by placing a rod across the top of the inverted cone and measuring the slump from the top center of the concrete mound to the bottom of the rod as shown in Figure 5.

Figure 5. Slump test.

4.5. Slump Flow Test

Another workability test performed in this study was the slump flow test described by ASTM C1611, Procedure A (88). Slump flow tests were conducted on a flat and level steel plate. The

slump cone was dampened and placed in the center of the steel plate, with the larger opening of the mold facing downward. After filling the mold in one lift, concrete was released from the cone by raising the cone vertically in 3 ± 1 secs. Then, the largest diameter of the resulting circular spread of concrete was measured after the concrete stopped flowing as shown in Figure 6. A second diameter of the circular spread was measured perpendicular to the original measured diameter. The average of these two dimeters was reported as the slump flow.

Figure 6. Slump flow test.

4.6. Compression Test

To identify UHPC mixtures, compressive strengths of all mixtures produced in this study with acceptable slump and slump flow values were evaluated using a 400,000-lbf (1780 kN) capacity universal testing machine. According to ASTM C1856 (1), mixtures with 28-day compressive strength greater than 17,000 psi (120 MPa) can be classified as acceptable UHPC. To assess compressive strengths of mixtures, three 3.94 in (100 mm) cube specimens from each mixture were removed from the moist room at ages of seven, 28, and 56 days and were tested for compressive strength according to BS1881 (89) as shown in Figure 7. After removing cubes from the moist room, the cubes were placed between high-yield strength steel platens to evenly distribute the compression load (platens were lightly oiled to decrease lateral confinement). According to BS1881 (89), cubes are to be tested at a load rate of 29 psi/s to 58 psi/s (0.2 MPa/s to 0.4 MPa/s). However, the load rate in this study was increased to 145 psi/s (1.0 MPa/s) as stated by ASTM C1856 (1). It should be noted that the reason for selecting cube specimens (instead of cylindrical specimens) for compression tests is that cubes do not require end preparation (grinding).

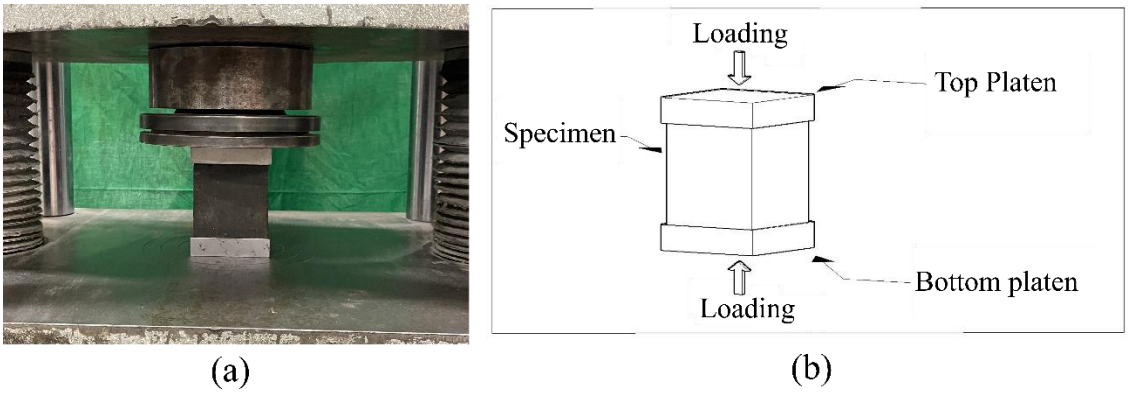

Figure 7. Compression test a) setup and b) schematic.

4.7. Flexural Test

To evaluate flexural strength properties, two 3×4×16 in (76×102×406 mm) prism specimens from each mixture with acceptable slump and slump flow values were evaluated according to the flexural test described in ASTM C1609 (90) using a 400,000-lbf (1780 kN) capacity universal testing machine (Figure 8).

Figure 8. Flexural test setup.

Specimens were placed on two semi-circular end supports located 2 in (51 mm) from each end of the specimen and then loaded with two concentrated loads, spaced 4 in (102 mm) apart, placed symmetrically about the midspan of the specimen. Two load cells (below supports), a string potentiometer at midspan, and two linear variable differential transformers (LVDTs) at 0.75 in (19 mm) from top and bottom surfaces of the specimen were used to measure the load, mid-span deflection, and displacements (used to compute strains) near the top and bottom of the specimens during flexural testing, as illustrated in Figure 9.

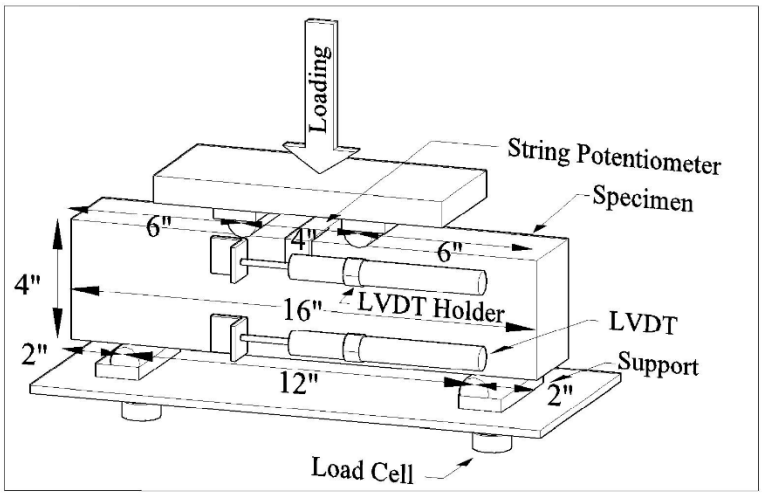

(a)

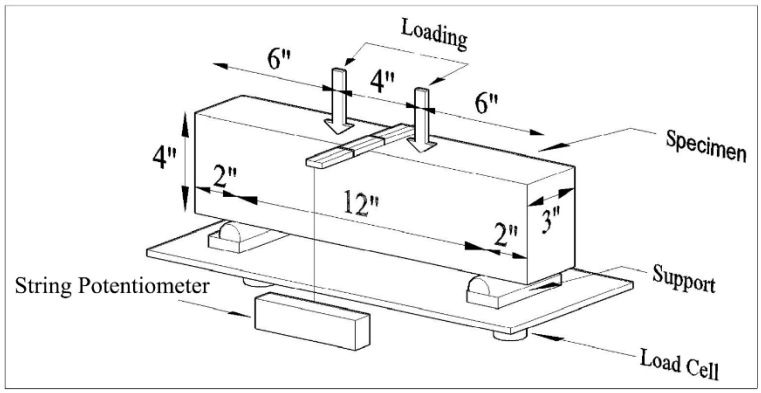

(b)

Figure 9. Schematic of flexural test a) front view and b) back view.

Modulus of rupture (MOR), peak strength (ultimate strength), residual strengths (including f_{600} and f_{150}), and toughness at 28 days were computed as described in ASTM C1609 (90). MOR was calculated as (90):

$$\mathrm{MOR} = \frac{\mathrm{P}\times\mathrm{L}}{\mathrm{b}\times\mathrm{d}^2} \qquad [5]$$

where P (local maximum load) is the load when the slope is zero on the load-deflection curve for the first time (lbf [N]), L is the span length (in [mm]), b is the width of the specimen (in [mm]), and d is the depth of the specimen (in [mm]).

Peak strength, f_{600}, and f_{150} were also calculated using Equation 5 with P being the greatest value of load prior to failure, P being the load at a net deflection of 1/600 of the span length, and P being the load at a net deflection of 1/150 of the span length, respectively.

4.8. Shrinkage

ASTM C157 (80) presents the most commonly used method to measure shrinkage in concrete specimens. The method specifies monitoring length changes using a length comparator. In this study, prism specimens with dimensions of 3×4×16 in (76×102×406 mm) were used for shrinkage testing to be consistent with freezing and thawing test specimens. Three specimens from each UHPC mixture were cured for 23.5 ± 0.5 hours before they were removed from the steel molds. After demolding, initial comparator readings were taken using the length comparator shown in Figure 10 and were then cured for 28 days in a moist room with relative humidity of 96% and temperature of 73±3°F (23±2°C). After the 28-day curing period, the specimens were removed from the moist room and the second length measurement was recorded. Specimens were then allowed to dry while stored at ambient conditions (relative humidity of 30±4 % and temperature of 68±3°F [20±2°C]) for an additional 28 days. Length comparator readings were recorded every three days for the 28-day drying period. Finally, average length changes for each UHPC mixture were used to compute shrinkage strains. During drying, specimens were stored with a clearance of at least 1.0 in (25 mm) on all sides. The relative humidity of 30% was less than the 50% recommended by ASTM C157 (80) and, therefore, provided conservative shrinkage results.

Figure 10. Shrinkage test.

4.9. Freezing and Thawing

To assess frost resistance of UHPC mixtures, freezing and thawing tests were performed on prismatic specimens according to ASTM C666, Procedure A (81). Three prismatic specimens from each UHPC mixture that measured 3×4×16 in. (76×102×406 mm) were subjected to six to seven freezing and thawing cycles per day in the freeze-thaw chamber shown in Figure 11. Each specimen was subjected to a total of 300 freezing and thawing cycles. A full freezing and thawing cycle consisted of rapidly decreasing the temperature from 40 to 0°F (4.4 to -17.8°C) in approximately two hours and 20 minutes and increasing the temperature from 0 to 40°F (-17.8 to 4.4°C) in approximately one hour and 20 minutes The temperature was held constant at 0°F (-17.8°C) for eight minutes at the bottom of the temperature cycle. At the top of the temperature cycle, the temperature was held constant at 40°F (4.4°C) for 10 minutes, except when specimens were being tested.

Figure 11. Freezing and thawing test.

Mass and fundamental transverse frequency measurements were taken at intervals that did not exceed 36 cycles. The recorded mass and frequency data were used to calculate the dynamic elastic modulus of the specimens according to ASTM C215 (82) using Equation 2.

Fundamental transverse frequencies were measured according to the impact resonance method described in ASTM C215 (82). For the impact resonance method, an instrumented hammer was used to excite a wide range of frequencies in the supported specimen and a lightweight accelerometer attached to the specimen was used to record the acceleration response history as shown in Figure 12. Fundamental frequency, resonant frequency for first mode vibration, was determined by identifying the frequency at which the maximum acceleration response occurs from a plot of amplitude versus frequency as shown in Figure 2.

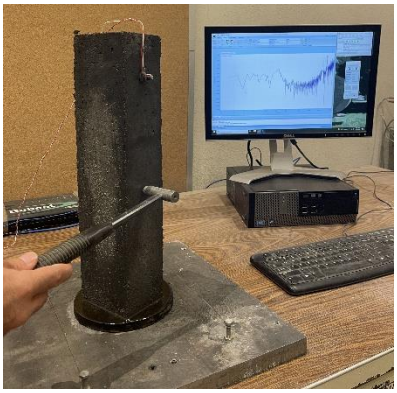

Figure 12. Fundamental transverse frequency test setup.

According to ASTM C215 (82), results from measurements obtained while monitoring deteriorating concrete should be presented in terms of the RDM computed using Equation 2.

After the freezing and thawing cycles were completed, Equation 6 was used to calculate the durability factor (DF):

$$DF = \frac{RDM \times N}{M} \qquad [6]$$

where N is the number of cycles and M is the specified number of cycles (300).

4.10. Rapid Chloride Permeability Test

To evaluate the chloride ion permeability of UHPC mixtures, RCPTs (ASTM C1202 [83]) were conducted after 56 days moist curing using two 2-in (51-mm) slices that were cut from two 4 by 8 in (102 by 203 mm) cylinder specimens from each UHPC mixture. The setup for the RCPT is shown in Figure 13. First, the slices were allowed to dry for one hour before a rapid setting coating was brushed on the circumferential surface of the specimens. Then, the slices were placed in a vacuum desiccator and the internal pressure was rapidly decreased to less than 0.96 psi (6650 Pa). The slices were then subjected to the vacuum pressure for three hours before being submerged in deionized water for one hour with the pump running. The specimens were kept in the vacuum desiccator for an additional 18 hours while the pump was off. After preparation, the specimens were placed in a testing cell with one side of a specimen exposed to a 3.0% sodium chloride (NaCl) solution and the other side of the specimen exposed to a 0.3 N sodium hydroxide (NaOH) solution. This test was performed using a 60V DC power supply to pass a current through the specimen that was measured every 30 minutes for six hours. Negative and positive terminals of the power supply were connected to the 3.0% NaCl solution and 0.3 N NaOH solution, respectively. Finally, the total charge passed (coulombs) was calculated using Equation 4.

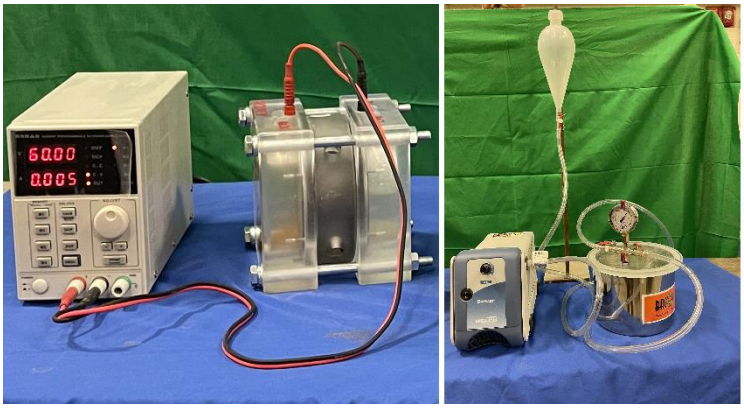

Figure 13. RCPT setup.

4.11. Surface Resistivity

The surface resistivity test is another permeability test conducted on all UHPC mixtures produced in this study to provide a rapid indication of chloride ion permeability for UHPC mixtures. In this study, 56-day surface resistivity tests were performed on three 4 by 8 in (102 by 203 mm) cylinders from each UHPC mixture using a four-pin Wenner probe array (Resipod Proceq) instrument, shown in Figure 14, according to AASHTO T 358 (84).

Figure 14. Surface resistivity test equipment.

5. FINDINGS

This chapter presents the results from mechanical and durability testing performed during this study. The tests that were conducted include slump, slump flow, compression and flexural strength tests, shrinkage measurements, freezing and thawing tests, RCPTs, and surface resistivity tests.

5.1. Workability

Table 6 presents slump and slump flow values for each mixture produced in this work. The 16 acceptable mixtures, with slump between 4 in (100 mm) and 8 in (205 mm) and slump flow between 8 in (205 mm) and 16 in (405 mm), are presented in bold font in Table 6. Workability of mixtures was consistent enough to achieve acceptable slump and slump flow values in no more than two attempts and only 27 trials were needed to produce 16 acceptable mixtures.

Table 6. Workability results.

Mixture Name	Trial No.	HRWRA gal/yd^3 (mL/m^3)	Slump in (mm)	Slump Flow in (mm)
S10-F10 (Control Mixture)	**Final**	**11.41 (56,500)**	**4.75 (120)**	**15.00 (380)**
	1st	9.10 (45,060)	2.50 (65)	12.50 (320)
S10-F5-N5	**Final**	**11.98 (59,330)**	**4.50 (115)**	**14.50 (370)**
	1st	11.41 (56,500)	3.75 (95)	14.00 (360)
S10-F2.5-N7.5	**Final**	**11.98 (59,330)**	**4.00 (100)**	**14.50 (370)**
S10-N10	**Final**	**12.55 (62,150)**	**4.00 (100)**	**14.50 (370)**
	1st	11.98 (59,330)	3.25 (85)	13.00 (330)
S10-F5-M5	**Final**	**13.12 (64,980)**	**5.00 (130)**	**15.00 (380)**
	1st	11.98 (59,330)	3.25 (85)	13.50 (340)
S10-F2.5-M7.5	**Final**	**13.12 (64,980)**	**4.50 (115)**	**14.50 (370)**
S10-M10	**Final**	**13.69 (67,800)**	**4.25 (110)**	**14.50 (370)**
	1st	13.12 (64,980)	3.50 (90)	13.50 (340)
S10-F8-G2	**Final**	**11.98 (59,330)**	**4.75 (120)**	**15.00 (380)**
	1st	11.41 (56,500)	3.75 (95)	14.00 (360)
S10-F6-G4	**Final**	**12.55 (62,150)**	**4.25 (110)**	**14.50 (370)**
	1st	11.98 (59,330)	3.50 (90)	13.50 (340)
S10-N5-M5	**Final**	**13.12 (64,980)**	**4.50 (115)**	**14.50 (370)**
	1st	12.55 (62,150)	3.50 (90)	13.50 (340)
S10-N2-M6-G2	**Final**	**13.69 (67,800)**	**4.25 (110)**	**14.00 (360)**
	1st	12.55 (62,150)	3.00 (75)	13.00 (330)
S9-M9-G2	**Final**	**13.69 (67,800)**	**4.00 (100)**	**14.00 (360)**
S9-M9-G12	**Final**	**13.12 (64,980)**	**5.00 (125)**	**15.00 (380)**
	1st	13.69 (67,800)	6.00 (150)	16.50 (420)
S7.5-N2.5-M10	**Final**	**12.55 (62,150)**	**4.50 (115)**	**14.50 (370)**
S7.5-M12.5	**Final**	**12.55 (62,150)**	**4.25 (110)**	**14.50 (370)**
	1st	13.69 (67,800)	6.00 (150)	16.50 (420)
S5-M15	**Final**	**12.55 (62,150)**	**5.25 (135)**	**15.50 (390)**

Results show that replacing fly ash with pumicite, metakaolin, and GGBFS increased HRWRA demand (decreased workability). This can be attributed to pumicite, metakaolin, and GGBFS being more angular than spherical fly ash particles. Replacing 100% of the fly ash in the control mixture with pumicite (S10-N10), replacing 100% of the fly ash in the control mixture with metakaolin (S10-M10), and replacing 40% of the fly ash in the control mixture with GGBFS (S10-F6-G4) increased HRWRA demand by 10.0, 20.0, and 10.0%, respectively. From these results, replacing 100% of the fly ash with pumicite increased HRWRA demand as much as replacing 40% of the

fly ash with GGBFS to produce acceptable slump and slump flow values, indicating that GGBFS decreased workability more than pumicite. Additionally, mixtures containing metakaolin required more HRWRA to produce acceptable slump and slump flow values than mixtures containing pumicite. Since workability of UHPC mixtures is sensitive to the particle size (specific surface area) and shape of ingredients, ultra-fine metakaolin with smaller particles (greater specific surface area) than pumicite have greater water demand that leads to an increase in HRWRA demand.

Results from mixtures S9-M9-G2 and S9-M9-G12 show that replacing 10% of the cement in mixture S9-N9-G2 with GGBFS reduced HRWRA demand. A possible explanation for this is slower water consumption by GGBFS than by cement during hydration. Similarly, comparing mixtures S7.5-N2.5-M10, S7.5-M12.5, and S5-M15 with mixture S10-M10 shows that replacing silica fume with either pumicite or metakaolin decreased HRWRA demand. This is attributed to the silica fume particles being smaller and requiring more water due to their greater surface area than pumicite and metakaolin particles.

5.2. Compressive Strength

Average compressive strengths for three specimens from each mixture tested at seven, 28, and 56 days are presented in Table 7 and Figure 15. Mixtures S10-N10, S9-M9-G12, and S5-M15 did not produce 28-day compressive strengths greater than 17,000 psi (120 MPa), which is a requirement for UHPC based on ASTM C1856 (1). However, the 56-day strengths for these three mixtures were greater than 20,020 psi (138.0 MPa), which should be suitable for many UHPC applications, indicating that a more liberal definition of UHPC could capture the longer-term benefit provided by the natural pozzolan, metakaolin, or GGBFS.

Results from compression tests indicate that replacing fly ash with any of the SCMs used in this study decreased seven-day compressive strength, regardless of the amount of replacement. The greatest reduction in seven-day strength (12.6%) occurred when 100% of the fly ash in the control mixture was replaced with pumicite (S10-N10). Additionally, increasing the amount of replacement decreased seven-day compressive strength, showing that the SCMs used in this study react more slowly than fly ash in the first seven days. Seven-day results also showed that replacing silica fume with alternative SCMs (after replacing all of the fly ash with metakaolin) reduced compressive strengths. Replacing 25% of the silica fume with pumicite (S7.5-N2.5-M10), replacing 25% of the silica fume with metakaolin (S7.5-M12.5), and replacing 50% of the silica fume with metakaolin (S5-M15) reduced seven-day compressive strengths by 15.7, 17.5, 20.3%, respectively, compared to mixture S10-M10. Comparing these results with the results from replacing fly ash with pumicite or metakaolin shows that replacing 25 or 50% of the silica fume in the control mixture with pumicite or metakaolin reduced compressive strength more than replacing 100% of the fly ash in the control mixture with pumicite or metakaolin. This indicates that silica fume is a more reactive and vital component than fly ash in early-age strength development of UHPC mixtures.

Table 7. Compressive strength results.

Mixture	7-day Compressive strength psi (MPa)	28-day Compressive strength psi (MPa)	56-day Compressive strength psi (MPa)
S10-F10 (Control Mixture)	16,680 (115.0)	19,560 (135.0)	22,730 (156.5)
S10-F5-N5	15,130 (104.5)	19,120 (132.0)	22,690 (156.5)
S10-F2.5-N7.5	14,850 (102.5)	17,750 (122.5)	22,560 (155.5)
S10-N10	14,590 (100.5)	16,840 (116.0)	22,390 (154.5)
S10-F5-M5	15,760 (108.5)	19,460 (134.0)	21,980 (151.5)
S10-F2.5-M7.5	15,710 (108.5)	19,100 (131.5)	22,070 (152.0)
S10-M10	15,510 (107.0)	18,960 (130.5)	22,130 (152.5)
S10-F8-G2	16,310 (112.5)	19,480 (134.5)	22,960 (156.5)
S10-F6-G4	16,050 (110.5)	19,240 (132.5)	22,560 (155.5)
S10-N5-M5	14,860 (102.5)	17,870 (123.0)	22,200 (153.0)
S10-N2-M6-G2	15,670 (108.0)	19,030 (131.0)	22,090 (152.5)
S9-M9-G2	15,370 (106.0)	18,840 (130.0)	22,100 (152.5)
S9-M9-G12	13,130 (90.5)	16,140 (111.5)	21,440 (148.0)
S7.5-N2.5-M10	14,060 (97.0)	17,230 (119.0)	20,640 (142.5)
S7.5-M12.5	13,770 (95.0)	17,550 (121.0)	20,560 (142.0)
S5-M15	13,290 (91.5)	16,840 (116.0)	20,020 (138.0)

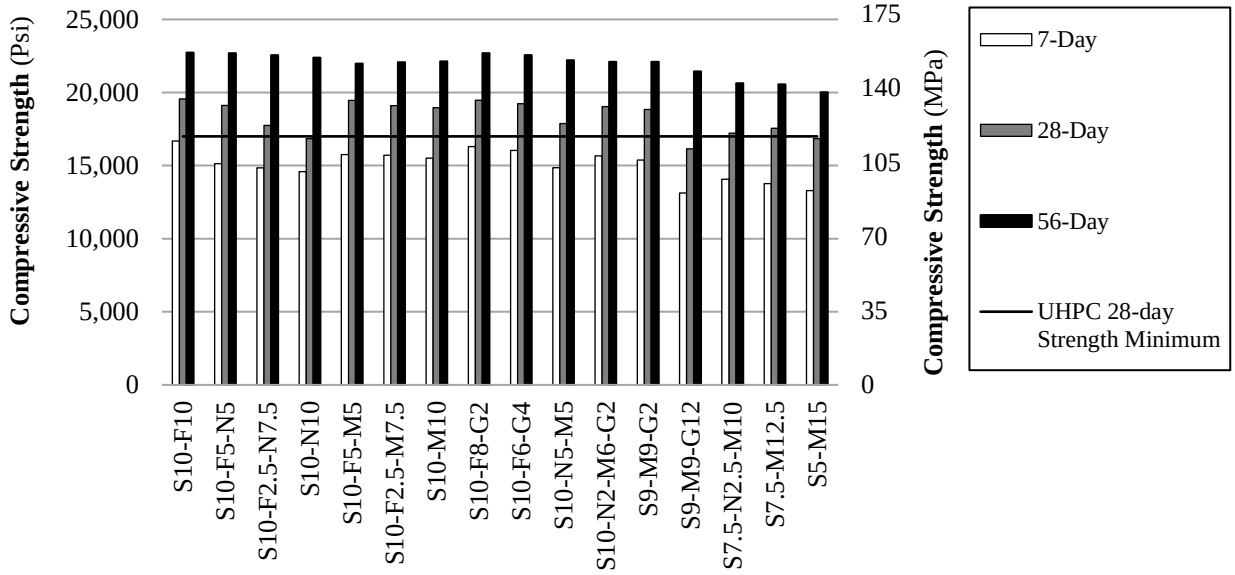

Figure 15. Compressive strength results.

Comparing 28-day compressive strength results show that replacing fly ash with pumicite, metakaolin, or GGBFS decreased 28-day strength (similar to seven-day tests results), however,

reductions in 28-day strengths caused by replacing fly ash (but not silica fume) with metakaolin were not as severe as reductions in seven-day strengths. Replacing 100% of the fly ash in the control mixture with pumicite (S10-N10) or metakaolin (S10-M10) decreased 28-day compressive strengths by 13.9 and 3.0%, respectively. This indicates that pumicite reacts more slowly than fly ash (similar to seven-day results) and that the slow reaction occurs for at least 28 days, which is consistent with Newtson et al. (91). However, at 28 days, the metakaolin reaction had essentially caught up with the reaction of the fly ash in the control mixture. Additionally, replacing 100% of the fly ash in the control mixture with 50% pumicite and 50% metakaolin reduced 28-day compressive strength by 8.6%, showing that the reaction of the pumicite and metakaolin was not rapid enough to catch up with the reaction of the fly ash in the first 28 days.

Comparing 28-day results for mixtures S7.5-N2.5-M10, S7.5-M12.5, and S5-M15 indicates that replacing 25% of the silica fume with pumicite, replacing 25% of the silica fume with metakaolin, and replacing 50% of the silica fume with metakaolin reduced 28-day compressive strengths by 11.9, 10.2, and 13.9%, respectively, compared to mixture S10-M10. As stated previously, replacing 100% of the fly ash in the control mixture with pumicite (S10-N10) or metakaolin (S10-M10) decreased 28-day compressive strength by 13.9 and 3.0%, respectively. Noting that replacing 25% of the silica fume with pumicite decreased 28-day compressive strength just slightly less than when 100% of the fly ash was replaced with pumicite (11.9% compared to 13.9%) and that replacing 25 or 50% of the silica fume with metakaolin decreased 28-day compressive strength more than replacing 100% of the fly ash with metakaolin indicate that silica fume is a more reactive and vital component than fly ash in 28-day strength development of UHPC mixtures. This observation is similar to what was observed in the seven-day tests.

Results from 56-day compressive strengths show that reductions in compressive strengths caused by replacing fly ash (but not silica fume) with alternative SCMs were of less magnitude than reductions at seven and 28 days. Mixtures S10-F6-G4, S10-N10, S10-M10, and S10-N5-M5 had 56-day compressive strength that were only 0.7, 1.5, 2.6, and 2.3% less than the control mixture, respectively. The greatest reduction (3.3%) occurred when 50% of the fly ash in the control mixture was replaced with metakaolin (S10-F5-M5). This shows that the pumicite, metakaolin, and GGBFS mixtures had comparable 56-day compressive strengths to that of the control mixture. As a reminder, GGBFS mixtures also had comparable compressive strengths to the control mixture at seven and 28 days and metakaolin mixtures had compressive strengths similar to the control mixture at 28 days. However, the fact that pumicite mixtures had comparable 56-day compressive strengths to the control mixture indicate that the pumicite reaction had finally progressed to the point that it was essentially equivalent to the fly ash reaction. This occurred because the pumicite was more reactive than fly ash after 28 days, which is consistent with previous research (91). It should be noted that due to the uncertain future availability of the fly ash, lower 28-day compressive strengths for pumicite mixtures may need to be accommodated to realize the long-term benefits of the natural pozzolan.

Although results from 56-day compression tests showed that replacing silica fume with pumicite or metakaolin decreased 56-day compressive strengths, mixtures with up to 50% replacement of silica fume had 56-day compressive strengths greater than 20,000 psi (137.9 MPa) indicating that long-term benefits of these mixtures are probably worth evaluating.

Comparing mixture S9-M9-G2 and mixture S9-M9-G12 shows that replacing 10% of the portland cement in mixture S9-M9-G2 with GGBFS (after full replacement of the fly ash and partial

replacement of the silica fume) reduced the seven-, 28-, and 56-day compressive strengths by 14.6, 14.3, and 3.0%, respectively. This shows that GGBFS is substantially less reactive than portland cement in the first 28 days and that GGBFS needs more time to produce compressive strengths comparable to the cement that it replaced.

5.3. Flexural Tests

Figure 16 shows a representative plot of load versus deflection from a flexural test in this study. UHPC reinforced with fibers is generally classified as strain-hardening fiber-reinforced concrete, which means fibers that bridge cracks provide post-cracking strength equal to or greater than the first-cracking strength *(3)*. In this study, the first crack occurred at point "A" causing load to decrease briefly. However, fibers bridging the initial crack allowed load to increase to the value at point "B" where the ultimate load occurs. After point "B", load remained elevated while substantial displacement continued to occur, which indicates substantial ductility and toughness in the UHPC.

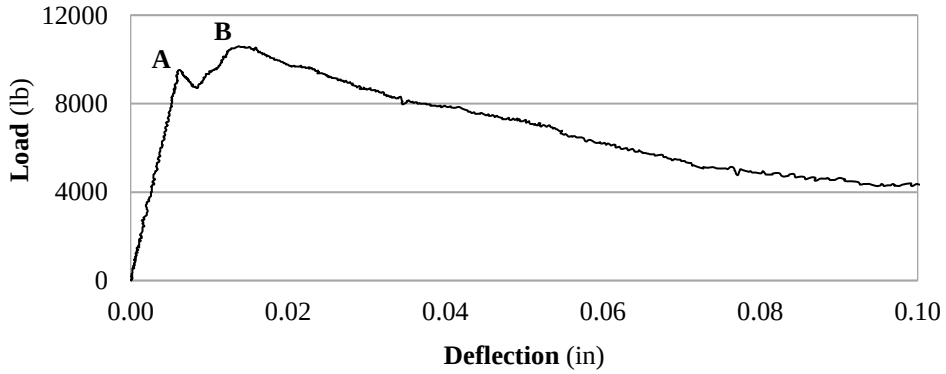

Figure 16. Load-deflection curve (mixture S10-F5-N5).

Table 8 presents average flexural properties from each mixture. In this work, all mixtures using pumicite, metakaolin, or GGBFS to replace fly ash (but not silica fume) had first peak (MOR) and peak strength (ultimate strength) values greater than 2685 psi (18.50 MPa) and 2800 psi (19.30 MPa), respectively, which were comparable to those for the control mixture (S10-F10). The greatest MOR and peak strength were obtained from mixture S10-N5-M5 where replacing 100% of the fly ash in the control mixture with a combination of pumicite and metakaolin increased MOR and peak strength values by 10.7 and 13.9%, respectively.

Table 8. Flexural strength results.

Mixture Name	MOR psi (MPa)	Peak Strength psi (MPa)	Residual Strength (f_{600}) psi (MPa)	Residual Strength (f_{150}) psi (MPa)	Toughness in-lb (J)
S10-F10 (Control Mixture)	2705 (18.65)	2835 (19.55)	2690 (18.55)	1575 (10.85)	590 (67)
S10-F5-N5	2910 (20.05)	3085 (21.25)	2950 (20.35)	1625 (11.20)	620 (70)
S10-F2.5-N7.5	2795 (19.25)	3020 (20.80)	2865 (19.75)	1605 (11.05)	620 (70)
S10-N10	2720 (18.75)	2900 (20.00)	2710 (18.70)	1475 (10.15)	590 (67)
S10-F5-M5	2825 (19.50)	3030 (20.90)	2910 (20.05)	1490 (10.25)	600 (68)
S10-F2.5-M7.5	2785 (19.20)	2975 (20.50)	2840 (19.60)	1445 (9.95)	590 (67)
S10-M10	2735 (18.85)	2960 (20.40)	2825 (19.50)	975 (6.70)	560 (63)
S10-F8-G2	2700 (18.60)	2825 (19.50)	2675 (18.45)	1550 (10.70)	590 (67)
S10-F6-G4	2685 (18.50)	2800 (19.30)	2600 (17.95)	1490 (10.25)	580 (66)
S10-N5-M5	2995 (20.65)	3230 (22.25)	3165 (21.80)	1700 (11.70)	660 (75)
S10-N2-M6-G2	2830 (19.50)	3065 (21.15)	2935 (20.25)	1540 (10.60)	640 (72)
S9-M9-G2	2815 (19.40)	3025 (20.85)	2905 (20.50)	1385 (9.55)	600 (68)
S9-M9-G12	2455 (16.95)	2610 (18.00)	2430 (16.75)	1370 (9.45)	530 (60)
S7.5-N2.5-M10	2280 (15.70)	2465 (17.00)	2365 (16.30)	1330 (9.15)	500 (56)
S7.5-M12.5	2245 (15.50)	2380 (16.40)	2185 (15.05)	1290 (8.90)	460 (52)
S5-M15	2060 (14.20)	2185 (15.05)	1980 (13.65)	875 (6.05)	430 (49)

However, increasing pumicite content from 5 to 10% in mixtures S10-F5-N5, S10-F2.5-N7.5, and S10-N10 reduced MOR and peak strength values by 6.5 and 6.0%, respectively. Similarly, comparing mixtures S10-F5-M5, S10-F2.5-M7.5, and S10-M10 indicates that increasing metakaolin content from 5 to 10% slightly decreased MOR and peak strength values by 3.2 and 2.3%, respectively. Additionally, increasing GGBFS content from 2 to 4% in mixtures S10-F8-G2 and S10-F6-G4 decreased MOR and peak strength values by 0.6 and 0.9%, respectively. The residual strengths (f_{600} and f_{150}) present similar trends to those presented by MOR and peak strength. This trend of decreasing MOR, peak, and residual strengths values with increasing pumicite, metakaolin, and GGBFS contents is consistent with the trend observed for 28-day compressive strengths. However, MOR and peak strength of the pumicite, metakaolin, and GGBFS mixtures were still comparable to the control (fly ash) mixture. This shows that pumicite, metakaolin, and GGBFS can be promising alternatives for fly ash in terms of flexural strength.

Replacing silica fume with alternative SCMs (after replacing 100% of the fly ash) significantly reduced MOR and peak strength values. Replacing 25% of the silica fume with pumicite (S7.5-N2.5-M10), replacing 25% of the silica fume with metakaolin (S7.5-M12.5), and replacing 50% of the silica fume with metakaolin (S5-M15), by modifying the proportions from mixture S10-M10, reduced MOR values by 16.6, 17.9, and 24.7%, respectively. Additionally, the reductions for peak strength were 16.7, 19.6, and 26.2%, respectively. Although the MOR and peak strength values for mixtures S7.5-N2.5-M10, S7.5-M12.5, and S5-M15 were greater than 2000 psi (13.80 MPa), which should be considered an acceptable flexural strength for UHPC, these relatively large reductions in MOR and peak strength should be considered when attempting to replace silica fume in UHPC mixture proportions.

Replacing 10% of the portland cement in mixture S9-M9-G2 with GGBFS, after full replacement of the fly ash and partial replacement of the silica fume in the control mixture with a combination of metakaolin and GGBFS, to produce mixture S9-M9-G12 reduced MOR and peak strength

values by 12.8 and 13.3%, respectively. This indicates that replacing portland cement with GGBFS in UHPC mixtures should be implemented with caution.

Overall, replacing 100% of the fly ash with either pumicite, metakaolin, or a combination of pumicite and metakaolin improved MOR and peak strength while providing comparable toughness, indicating that these SCMs appear to be suitable replacements for fly ash. However, replacing 25 or 50% of the silica fume (after replacing all of the fly ash) with either pumicite or metakaolin as well as replacing 10% of the portland cement with GGBFS (after replacing all of the fly ash and 10% of the silica fume) substantially decreased MOR, peak strength, and toughness, indicating that flexural strength should be considered when replacing silica fume or portland cement with alternative SCMs in UHPC.

5.4. Shrinkage

Table 9 and Figure 17 present average 28- and 56-day shrinkage results of three prisms from each UHPC mixture. Immediately after demolding, shrinkage monitoring was initiated and continued for 56 days (28 days of moist curing followed by 28 days of air curing). Results indicated that the greatest shrinkage occurred in mixture S10-F6-F4 where 28- and 56-day shrinkage values were 312 μstrain and 406 μstrain, respectively, showing that all of the UHPC mixtures had shrinkage values less than the maximum permissible value of 500 μstrain that is acceptable to many transportation agencies. The fact that the UHPC mixtures produced in this study had little susceptibility to shrinkage is consistent with observations from other researchers (*46, 91*). Since UHPC mixtures contain high cementitious materials content, it was expected that shrinkage values would be greater than what were observed in this study. However, it appears that steel fibers provide internal restraint and the low w/cm causes incomplete hydration of the cementitious materials which led to the limited shrinkage.

Table 9. Shrinkage test results.

Mixture	**28-day Shrinkage** (μstrain)	**56-day Shrinkage** (μstrain)
S10-F10 (Control Mixture)	270	371
S10-F5-N5	242	317
S10-F2.5-N7.5	223	290
S10-N10*	NA	NA
S10-F5-M5	231	286
S10-F2.5-M7.5	190	242
S10-M10	198	229
S10-F8-G2	293	377
S10-F6-G4	312	406
S10-N5-M5	185	215
S10-N2-M6-G2	198	248
S9-M9-G2	202	238
S9-M9-G12*	NA	NA
S7.5-N2.5-M10	229	273
S7.5-M12.5	217	260
S5-M15*	NA	NA

* Not tested since the mixture did not meet UHPC requirements.

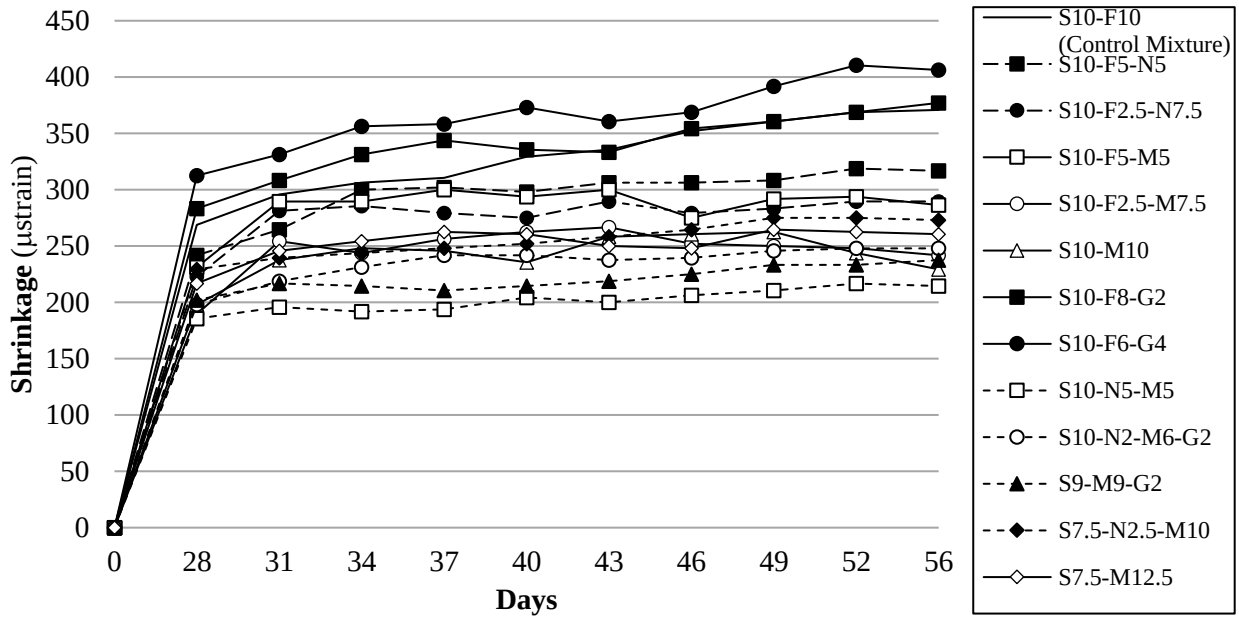

Figure 17. Shrinkage test results.

Results also showed that replacing 75% of the fly ash in the control mixture with pumicite (S10-F2.5-N7.5), replacing 100% of the fly ash in the control mixture with metakaolin (S10-M10), and replacing 100% of the fly ash in the control mixture with a combination of pumicite and metakaolin (S10-N5-M5) reduced 56-day shrinkage by 21.8, 38.3, and 42.0%, respectively. Additionally, increasing pumicite from 5 to 7.5% in mixtures S10-F5-N5 and S10-F2.5-N7.5 or increasing metakaolin from 5 to 10% in mixtures S10-F5-M5, S10-F2.5-M7.5, and S10-M10 decreased shrinkage. These trends can be attributed to pumicite and metakaolin particles being much smaller (greater surface area) than fly ash particles (Table 4) and causing greater refinement of the capillary pores that reduces drying shrinkage by obstructing evaporation of capillary water (46). Another mechanism to reduce shrinkage is the slow reactivity of the pumicite that can delay shrinkage until the skeletal structure has formed and helps restrain shrinkage.

Replacing 40% of the fly ash in the control mixture with GGBFS (S10-F6-G4) increased 28- and 56-day shrinkage by 15.6 and 9.4%, respectively. This can be attributed to GGBFS being more angular and slightly larger than the spherical fly ash particles, which can lead to less refinement of the capillary pores. These results also show that the relative increase in shrinkage caused by using GGBFS decreases with time.

Comparing mixtures S7.5-N2.5-M10 and S7.5-M12.5 with mixture S10-M10 shows that adding pumicite or more metakaolin to replace 25% of the silica fume in the control mixture (after replacing all of the fly ash in the control mixture with metakaolin to produce mixture S10-M10) increased 56-day shrinkage by 19.2 and 13.5%, respectively. This indicates that replacing silica fume with pumicite or metakaolin increases shrinkage, which is consistent with arguments from other researchers that silica fume with smaller particles (greater surface area) than pumicite and metakaolin is better for limiting shrinkage by filling capillary pores and blocking pathways for evaporating capillary water (46).

5.5. Freezing and Thawing

Results for freezing and thawing tests are presented in Table 10 and Figure 18. The results show that DF for all UHPC mixtures were greater than 105 and the greatest DF values (109) were produced by mixtures S10-M10 and S10-N5-M5. This shows that all of the UHPC mixtures were resistant to degradation caused by freezing and thawing cycles, regardless of SCM type. Other researchers have also shown that UHPC has excellent resistance to freezing and thawing (92).

The results also show that RDM values increased slightly during the freezing and thawing cycles which can be attributed to specimens containing un-hydrated cementitious materials that were able to react throughout the duration of the test causing an increase in dynamic modulus (*3, 92*). However, RDM values for all UHPC mixtures were comparable and replacing fly ash or silica fume in the control mixture with pumicite, metakaolin, GGBFS, or a combination of these SCMs did not significantly change the RDM and DF values. This shows that pumicite, metakaolin, and GGBFS all appear to be suitable replacements for fly ash and silica fume in terms of frost resistance.

Table 10. Freezing and thawing test results.

Mixture	DF (300-cycle RDM)
S10-F10 (Control Mixture)	105
S10-F5-N5	106
S10-F2.5-N7.5	106
S10-N10*	NA
S10-F5-M5	106
S10-F2.5-M7.5	107
S10-M10	109
S10-F8-G2	105
S10-F6-G4	106
S10-N5-M5	109
S10-N2-M6-G2	106
S9-M9-G2	107
S9-M9-G12*	NA
S7.5-N2.5-M10	107
S7.5-M12.5	106
S5-M15*	NA

* Not tested since the mixture did not meet UHPC requirements.

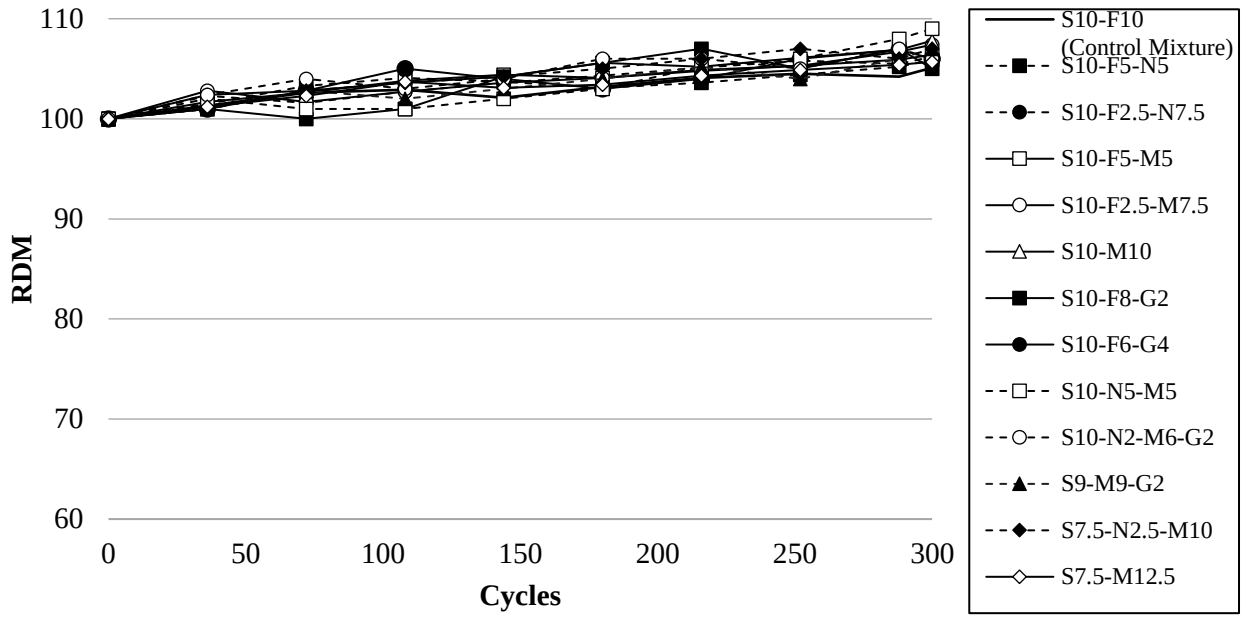

Figure 18. Freezing and thawing test results.

5.6. Rapid Chloride Permeability Test

Chloride ion permeability of each UHPC mixture was evaluated with RCPTs at 56 days since ASTM C1202 (83) recommends a minimum of 56-day moist curing prior to performing RCPTs on specimens containing SCMs. This is because testing at 56 days allows slow reacting SCMs to react more completely and provides a better indication of the long-term chloride ion permeability of concrete mixtures containing SCMs. Average 56-day RCPT results from each UHPC mixture are presented in Table 11 and Figure 19. RCPT results showed that total charge passed for all UHPC mixtures were in the range of 119 to 165 coulombs. All these RCPT results indicate "very low" chloride ion penetration since they are between 100 and 1000 coulombs (83).

Table 11. RCPT results.

Mixture	**Total Charge Passed** (Coulombs)	**Coefficient of Variation** (%)
S10-F10 (Control Mixture)	165	2.2
S10-F5-N5	142	2.6
S10-F2.5-N7.5	136	1.4
S10-N10*	NA	NA
S10-F5-M5	135	0.9
S10-F2.5-M7.5	124	1.5
S10-M10	119	2.1
S10-F8-G2	162	1.1
S10-F6-G4	155	2.0
S10-N5-M5	122	1.5
S10-N2-M6-G2	121	2.0
S9-M9-G2	125	2.4
S9-M9-G12*	NA	NA
S7.5-N2.5-M10	162	1.5
S7.5-M12.5	160	0.8
S5-M15*	NA	NA

* Not tested since the mixture did not meet UHPC requirements.

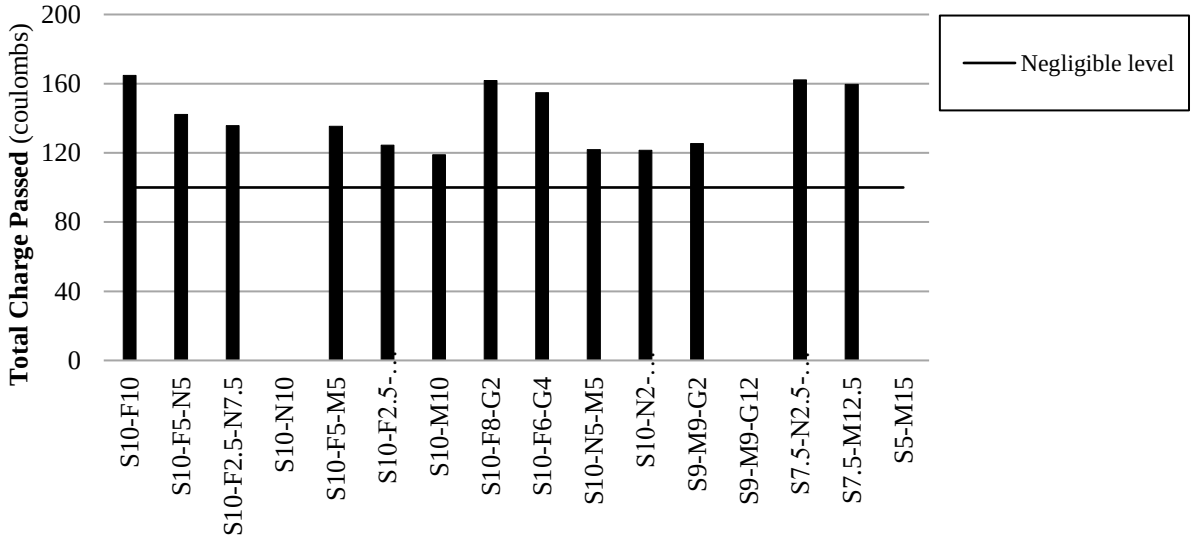

Figure 19. RCPT results.

Generally, replacing fly ash with any of the alternative SCMs in this study decreased total charge passed (chloride ion permeability). Replacing 75% of the fly ash in the control mixture with pumicite (S10-F2.5-N7.5), with metakaolin (S10-F2.5-M7.5), or replacing 40% of the fly ash in the control mixture with GGBFS (S10-F6-G4) decreased chloride ion permeability by 17.6, 24.8, and 6.1%, respectively. However, the greatest reductions in total charge passed was produced by mixtures S10-M10 (27.9%), S10-N2-M6-G2 (26.7%), and S10-N5-M5 (26.0) when all of the fly ash in the control mixture was replaced with metakaolin or a combination of pumicite, metakaolin, and GGBFS. These results are consistent with observations of pumicite and metakaolin causing reduced chloride ion permeability by other researchers (*46*, *91*, *93*) that attribute the reduced chloride ion permeability to the SCMs forming additional secondary CSH as well as the fineness of pumicite and metakaolin particles filling pore space that leads to lower permeability.

Increasing pumicite content from 5 to 7.5% (in mixtures S10-F5-N5 and S10-F2.5-N7.5), increasing metakaolin content from 5 to 7.5% (in mixtures S10-F5-M5 and S10-F2.5-M7.5), and increasing GGBFS content from 2 to 4% (in mixtures S10-F8-G2 and S10-F6-G4) reduced total charge passed by 4.2, 8.1, and 4.3%, respectively, indicating that metakaolin appeared to be more effective than pumicite and GGBFS at improving chloride ion penetration resistance. This is attributed to the metakaolin particles being finer than the fly ash, pumicite, and GGBFS particles which facilitates a more refined pore system.

After replacing all of the fly ash in the control mixture with metakaolin, replacing 25% of the silica fume in the control mixture with pumicite (S7.5-N2.5-M10) or metakaolin (S7.5-M12.5) increased total charge passed to 162 and 160 coulombs, respectively, compared to 119 coulombs for mixture S10-M10. This indicates that replacing silica fume with pumicite or metakaolin increased chloride ion penetration, most likely due to the pumicite and metakaolin particles being larger than silica fume particles (Table 4) and producing less refined capillary pores (46). Overall, the results show that pumicite (natural pozzolan), metakaolin, and GGBFS appear to have the potential to partially or completely replace fly ash and silica fume in UHPC mixtures in terms of chloride ion permeability.

It should be noted that ASTM C1202 (83) warns that specimens containing steel fibers or other embedded electrically conductive materials may produce erroneous RCPT results with high total charge passed. However, the low values obtained in this research (less than 165 coulombs) indicate that it is unlikely that a conductive path was created between the two ends of the specimens used in this study. Other researchers have also reported that steel fibers in UHPC are generally discontinuous and do not provide a direct path to complete an electric circuit (3).

5.7. Surface Resistivity

Surface resistivity tests were also performed on UHPC mixtures at 56 days. Average 56-day surface resistivity test results are presented in Table 12 and Figure 20 and ranged between 15.2 kΩ-in (386 kΩ-mm) and 23.7 kΩ-in (603 kΩ-mm), indicating that the chloride ion penetration for all of the UHPC mixtures were "very low" according to AASHTO T 358 (84). These results matched well with the RCPT results where all of the UHPC mixtures were classified as having "very low" chloride ion penetration, which is also consistent with other researchers (*46, 91*). Similar to ASTM C1202 (83), AASHTO T 358 (84) states that the presence of steel fibers or other embedded electrically conductive materials may significantly decrease surface resistivity. However, since relatively large surface resistivity values were obtained (greater than 15.2 kΩ-in [386 kΩ-mm]) and the results were consistent with the RCPT results, it appears that the steel fibers were adequately dispersed and discontinuous so that there were no conductive paths between the Wenner probe pins.

Table 12. Surface resistivity results.

Mixture	**Surface Resistivity** kΩ-in **(**kΩ-mm**)**	**Coefficient of Variation** (%)
S10-F10 (Control Mixture)	15.2 (386)	14.8
S10-F5-N5	16.7 (424)	20.8
S10-F2.5-N7.5	18.2 (463)	14.4
S10-N10*	NA	NA
S10-F5-M5	17.2 (437)	16.8
S10-F2.5-M7.5	20.5 (520)	18.9
S10-M10	23.7 (603)	8.7
S10-F8-G2	15.6 (395)	14.5
S10-F6-G4	16.2 (412)	13.1
S10-N5-M5	18.0 (458)	15.9
S10-N2-M6-G2	17.0 (431)	16.1
S9-M9-G2	23.0 (584)	13.8
S9-M9-G12*	NA	NA
S7.5-N2.5-M10	17.1 (435)	14.2
S7.5-M12.5	17.3 (440)	10.2
S5-M15*	NA	NA

* Not tested since the mixture did not meet UHPC requirements.

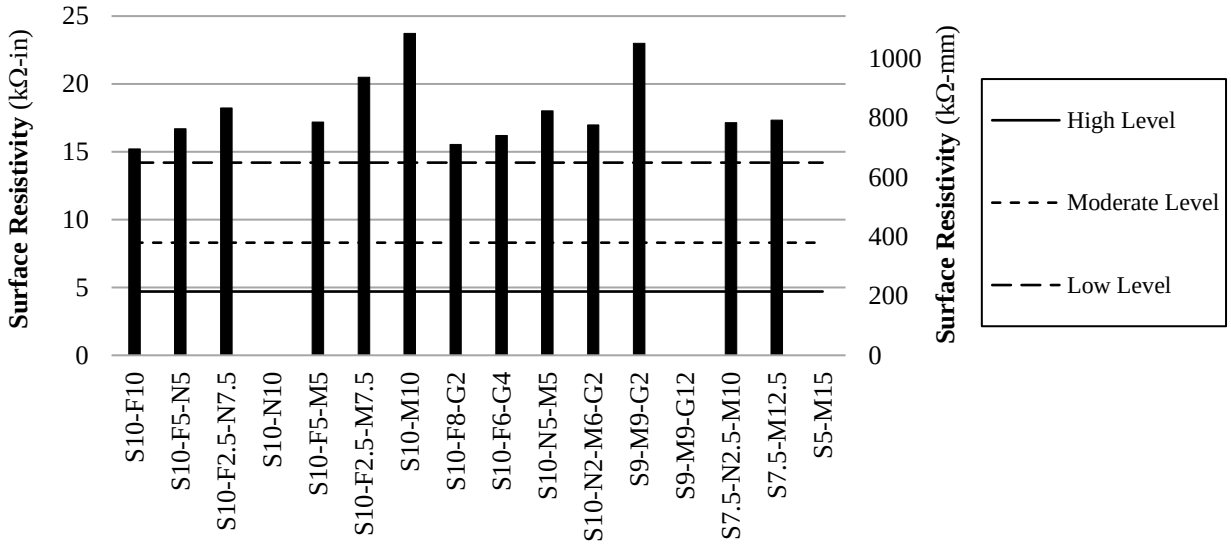

Figure 20. Surface resistivity test results.

Similar to RCPT results, replacing fly ash with any of the alternative SCMs used in this study increased surface resistivity (decreased chloride ion permeability). However, the greatest improvement in chloride ion permeability occurred when all of the fly ash in the control mixture was replaced with metakaolin (S10-M10) with a surface resistivity value of 23.7 kΩ-in (603 kΩ-mm).

Increasing pumicite content from 5 to 7.5% in mixtures S10-F5-N5 and S10-F2.5-N7.5, increasing metakaolin content from 5 to 7.5% in mixtures S10-F5-M5 and S10-F2.5-M7.5, and increasing GGBFS content from 2 to 4% in mixtures S10-F8-G2 and S10-F6-G4 increased surface resistivity by 9.0, 19.2, and 3.8%, respectively, indicating that pumicite, metakaolin and GGBFS can improve resistance to chloride ion penetration which is consistent with the RCPT results. Increasing resistance to chloride ion penetration with increasing pumicite, metakaolin, and GGBFS content is attributed to the greater density and refined capillary pores caused by fine particles of pumicite, metakaolin, and GGBFS compared to the fly ash (46). Similar to the RCPT results, metakaolin was more beneficial than pumicite due to the metakaolin particles being smaller than pumicite particles (Table 4).

Comparing mixtures S7.5-N2.5-M10 and S7.5-M12.5 with mixture S10-M10 shows that replacing 25% of the silica fume in mixture S10-M10 with pumicite or metakaolin (having already replaced all of the fly ash with metakaolin) reduced surface resistivity by 27.8 and 27.0%, respectively. This indicates that replacing silica fume with pumicite or metakaolin increased chloride ion penetration, which is also consistent with the RCPT results. Increasing chloride ion penetration with decreasing silica fume content is again attributed to the larger pumicite and metakaolin particles (than silica fume) producing less refined capillary pores (46).

5.8. RCPT and Surface Resistivity Test comparison

RCPT and surface resistivity test results consistently indicated that replacing fly ash with pumicite, metakaolin, or GGBFS decreased permeability while replacing silica fume with pumicite or metakaolin increased permeability. This consistency between the RCPT and surface resistivity test

results, in combination with the results being consistent with results from other researchers, show that both tests appear to be valid for assessing chloride ion permeability of UHPC containing steel fibers. However, the coefficients of variation for the surface resistivity test results (Table 12) were much greater than the maximum permissible value of 6.3% specified by AASHTO T 358 (84) for a single operator, while coefficients of variation for the RCPT results (Table 11) were acceptable according to ASTM C1202 (83). The high variation for the surface resistivity tests was most likely caused by the steel fibers, however, additional research would be need to performed to verify this.

Comparing the RCPT and surface resistivity tests also shows that the surface resistivity test has several advantages. These advantages include:

1. A surface resistivity test takes approximately 30 minutes to perform, whereas a RCPT requires approximately 30 hours to pre-condition a sample and run the test.
2. Surface resistivity tests can be conducted in-situ, while the RCPT requires a sample to be cut from a concrete specimen or member and the test can only be performed under laboratory conditions.
3. Surface resistivity can be measured at low voltages, and this voltage is only applied for brief periods. This avoids errors resulting from heating of the concrete that can occur during a RCPT (94).

6. CONCLUSIONS

Based on the research conducted during the course of this project, the following conclusions were drawn:

1. Workability of all mixtures containing pumicite, metakaolin, or GGBFS was consistent enough to achieve the targeted workability in no more than two attempts.
2. Pumicite was able to replace up to 75% of the fly ash in the control mixture and metakaolin was able to replace up to 100% of the fly ash and 25% of the silica fume in the control mixture while producing 28-day compressive strengths greater than 17,000 psi (120 MPa). However, replacing 10% of the cement with GGBFS did not produce acceptable compressive strength.
3. Mixtures with low 28-day compressive strength (less than 17,000 psi [120 MPa]) had 56-day compressive strengths that were greater than 20,000 psi (137.9 MPa) indicating that lower 28-day compressive strengths may need to be accommodated to realize the long-term benefits of some alternative SCMs.
4. All specimens containing pumicite, metakaolin, or GGBFS as a replacement for fly ash or silica fume had toughness values greater than 430 in-lb (49 J) and flexural strengths greater than 2000 psi (13.80 MPa), which should be considered acceptable for UHPC.
5. All UHPC mixtures produced in this study had little susceptibility to shrinkage, as indicated by 56-day shrinkage values that were no greater than 406 μstrain.
6. All UHPC mixtures had DF values of at least 105 after 300 cycles of freezing and thawing, indicating that UHPC mixtures produced in this study were extremely resistant to freezing and thawing.
7. RCPT and surface resistivity test results were similar and showed that chloride ion penetration for all UHPC mixtures was “very low.”
8. Increasing pumicite, metakaolin, and GGBFS contents to replace fly ash (not silica fume) decreased drying shrinkage and chloride ion penetration.
9. After replacing 100% of the fly ash in the control mixture with alternative SCMs, a further increase in pumicite or metakaolin content to replace silica fume resulted in increased drying shrinkage and chloride ion penetration, most likely due to unrefined capillary pore systems produced by pumicite and metakaolin particles that were larger than the silica fume particles.
10. Overall, the results showed that pumicite (natural pozzolan), metakaolin, and GGBFS can be incorporated into UHPC mixtures to replace fly ash without substantial loss of strength and can even improve durability characteristics such as shrinkage, frost resistance, and permeability.
11. Mixtures using pumicite or metakaolin to partially replace silica fume (after replacing all of the fly ash with metakaolin) had better durability properties than the control mixture but showed decreasing durability and strengths properties with decreasing silica fume content.

REFERENCES

1. ASTM C1856/M-17: Standards *Practice for Fabricating on Testing Specimens of UHPC*. Annual Book of ASTM Standards. ASTM International, West Conshohocken, PA, 2017.
2. American Coal Ash Association (ACAA). Fly Ash Use in Concrete Increases Slightly as Overall Coal Ash Recycling Rate Declines. Retrieved on July 2022 from https://acaa-usa.org.
3. Graybeal, B. Ultra-High Performance Concrete. Publication No. FHWA-HRT-11-038. FHWA, U.S. Department of Transportation, 2011.
4. Hussein, H., S. Sargand, and E. Steinberg. Shape Optimization of UHPC Shear Keys for Precast, Prestressed, Adjacent Box-Girder Bridges. *ASCE Journal of Bridge Engineering*, 2018. 23(4): 1–5.
5. Wille, K., S. El-Tawil, and A. E. Naaman. Properties of Strain Hardening Ultra High Performance Fiber Reinforced Concrete (UHP-FRC) Under Direct Tensile Loading. *Cement and Concrete Composites*, 2014. 48: 53–66.
6. Wille, K., and C. Boisvert-Cotulio. Material Efficiency in the Design of Ultra-High Performance Concrete. *Construction and Building Materials*, 2015. 86: 33–43.
7. Al-Basha, A. Frost Resistance of Concrete Cladded with Locally Produced Ultra-High-Performance Concrete Cured at Elevated Temperatures. *M.S. thesis*. New Mexico State University, 2017.
8. Magureanu, C., I. Sosa, C. Negrutiu, and B. Heghes. Mechanical Properties and Durability of Ultra-High-Performance Concrete. *American Concrete Institute (ACI) Materials Journal*, 2012. 109(2): 177–183.
9. Richard, P., and M. Cheyrezy. Composition of Reactive Powder Concretes. *Cement and Concrete Research*, 1995. 25(7): 1501–1511.
10. Villanueva, J. M. Mixture Proportioning and Freezing and Thawing Durability of Ultra High Performance Concrete Using Local Materials. *Ph.D. dissertation*, New Mexico State University, 2015.
11. Way, R., and K. Wille. Material Characterization of an Ultra High-Performance-Fibre Reinforced Concrete under Elevated Temperatures. *Third International Symposium on UHPC and Nanotechnology for High Performance Construction Materials*, Kassel, 2012. pp. 565–572.
12. Graybeal, B., and J. Tanesi. Durability of an Ultrahigh-Performance Concrete. *Journal of Materials in Civil Engineering*, 2007. 19: 848–854.
13. Shi, C., Z. Wu, J. Xiao, D. Wang, Z. Huang, Z. Fang. A review on ultra-High performance concrete: part I. Raw materials and mixture design. *Construction and Building Materials*, 2015. 101(1): 741–751.
14. Buck, J. J., D. L. McDowell, and M. Zhou. Effect of microstructure on load carrying and energy dissipation capacities of UHPC. *Cement and Concrete Research*, 2013. 43: 34–50.

15. Azmee, N. M., and N. Shafiq. Ultra-high performance concrete: From fundamental to applications. Case Studies in Construction Materials, 2018. 9: e00197.

16. Acker, P., and M. Behloul. Ductal® technology: a large spectrum of properties, ultra-High performance concrete, Kassel. Germany, 2004. pp. 11–23.

17. Ubbing, J. Analytical Investigation of Adjacent Box Beam Ultra-High Performance Concrete Connections. *M.S. thesis*. Ohio University, 2014.

18. Allena, S., and C. M. Newtson, Shrinkage of Fiber-Reinforced Ultrahigh Strength Concrete. *Journal of Materials in Civil Engineering*, 2011. 24(5): 612–614.

19. Montoya, K. F. Feasibility of Using Ultra High Performance Concrete in New Mexico Bridge Girders. *M.S. thesis*. New Mexico State University, 2010.

20. Lyelle, E. Optimization of Ultra High Performance Concrete Mixture Proportions using Locally Available Materials. *M.S. thesis*. New Mexico State University, 2012.

21. Yigiter, H., S. Aydin, H. Yazici, and M. Y. Yardimci. Mechanical Performance of Low Cement Reactive Powder Concrete (LCRPC). *Composites Part B: Engineering*, 2012. 43: 2907–2914.

22. Bahmani, H., and D. Mostofinejad. Microstructure of Ultra-High-Performance Concrete (UHPC) – A Review Study. *Journal of Building Engineering*, 2022. 50: 104118.

23. Voo, Y. L., S. Foster, and L. G. Pek. Ultra-High Performance Concrete – Technology for Present and Future. *ACI Singapore*, Building Construction Authority Joint Seminar on Concrete for Sustainability, Productivity and The Future, 2017.

24. Blais, P. Y., and M. Couture. Precast, prestressed pedestrian Bridge - world's first reactive powder concrete structure. *PCI Journal*, 1999. 44(5): 60–71.

25. Maher, K. T., and Y. L. Voo. Taking ultra-high performance concrete to new height – the Malaysian experience. *Aspire the Concrete Bridge Magazine*, 2016. 36–38.

26. Resplendino, J., and F. Toutlemonde. The UHPFRC Revolution in Structural Design and Construction. *Proceedings of International Symposium on Ultra-High Performance Fiber-Reinforced Concrete*, 2013. 791–804.

27. Bruhwiler, E., and E. Denarie. Rehabilitation of concrete structures using ultra-High performance fiber reinforced concrete. *Proceedings of 2nd International Symposium on Ultra-High Performance Fiber-Reinforced Concrete*, 2008. 895–902.

28. Grunewald, S., H. Kohne, M. Nio, M. Serafini, A. Verdonk, R. Van Nalta, R. Huijben, V. Mechtcherine, L. Dudziak, and L. Gielbert. Optimization of a slender Bridge in UHPFRC. *Proceedings of International SympoSium on Ultra-High Performance Fiber-Reinforced Concrete*, 2013. 379–388.

29. Tirimanna, D., and J. Falbr. FDN modular UHPFRC Bridges. Proceedings of International Symposium on Ultra-High Performance Fiber-Reinforced Concrete, 2013. 395–404.

30. Naaman, A. E., and K. Wille. The path to ultra-High performance fiber reinforced concrete (UHP-FRC): Five decade of progress. *Proceedings of 3rd International Symposium on UHPC and Nanotechnology for High Performance Construction Materials,* 2012. 3–13.

31. Henry, G. A. Russell and Benjamin, and B. Graybeal. *Ultra-High Performance Concrete: A State-of-the-Art Report for The Bridge Community*. Publication No. FHWA-HRT-13-060. FHWA, U.S. Department of Transportation, 2013. 22101–22296.

32. Aaleti, S., S. Sritharan, D. Biewagen, and B. Moore. Precast UHPC waffle deck panels and connections for accelerated Bridge construction. *Proceedings of the PCI National Bridge Conference,* 2011.

33. Graybeal, B. *Ultra-High Performance Concrete for Bridge Deck Overlays*. Publication No. FHWA-HRT-17-097. FHWA, U.S. Department of Transportation, 2018.

34. Newtson, C. M., B. Weldon, E. Flores, J. Varbel, and W. Toledo. UHPC Shear Keys in Concrete Bridge Superstructures. *Final Research Report*, Tran-SET project 18CNMS01, Transportation Consortium of South-Central States, Louisiana State University, 2019.

35. Kosmatka, S. H., and M. L. Wilson. Design and Control of Concrete Mixtures. *Portland Cement Association (15th Edition),* 2011.

36. Soliman, N. A., A. Tagnit-Hamou. Partial substitution of silica fume with fine glass powder in UHPC: Filling the micro gap. *Construction and Building Materials,* 2017. 139: 374-383.

37. Sutter, L. L. *Supplementary Cementitious Materials - Best Practices for Concrete Pavements*. Publication No. FHWA-HIF-16-001. FHWA, U.S. Department of Transportation, 2016.

38. Malvar, L. J., and L. R. Lenke. Efficiency of Fly Ash in Mitigating Alkali-Silica Reaction Based on Chemical Composition. *American Concrete Institute (ACI) Materials Journal*, 2006, 103(5): 319–326.

39. Ahmed, T., M. Elchalakani, A. Karrech, and M. Dong. ECO-UHPC with High-Volume Class-F Fly Ash: New Insight into Mechanical and Durability Properties. Journal of Materials in Civil Engineering (ASCE), 2021. 33(7).

40. American Concrete Institute (ACI) Committee 116. *Cement and Concrete Terminology*. ACI 116R-00, Farmington Hills, Michigan, 2000.

41. ASTM C618-19: Standard Specification for Coal Fly Ash and Raw or Calcined Natural Pozzolan for Use in Concrete. Annual Book of ASTM Standards. ASTM International, West Conshohocken, PA, 2019.

42. Spears, D. A., J. H. Sharp, D. Thompson, and B. B. Argent. Prediction of the Phases Present in Fly Ash, Their Composition and the Influence of These Factors on Its Utility and Disposal. *Proceedings of The Institute of Energy Conference*, London, UK, December 1995. 71–87.

43. Sudarsan, V. Materials Under Extreme Conditions, Elsevier, ISBN: 9780128013007. Chapter 4 - *Materials for Hostile Chemical Environments,* 2017. 129–158.

44. Khandaker, M., and A. Hossain. Properties of Volcanic Pumice Based Cement and Lightweight. *Cement and Concrete Research*, 2004. 34(2): 283–291.

45. Al-Chaar, G. K., M. Alkadi, and P. G. Asteris. Natural Pozzolan as a Partial Substitute for Cement in Concrete. *The Open Construction and Building Technology Journal*, 2013. 7: 33–42.

46. Ahmad, S., K. O. Mohaisen, S. K. Adekunle, S. U. Al-Dulaijan, and M. Maslehuddin. Influence of Admixing Natural Pozzolan as Partial Replacement of Cement and Microsilica in UHPC Mixtures. *Construction and Building Materials*, 2019. 198: 437–444.

47. Sarıdemir, M. Effect of Silica Fume and Ground Pumice on Compressive Strength and Modulus of Elasticity of High Strength Concrete. *Construction and Building Materials*, 2013. 49: 484–489.

48. Zeyad, A. M., B. A. Tayeh, and M. O. Yusuf. Strength and Transport Characteristics of Volcanic Pumice Powder Based High Strength Concrete. *Construction and Building Materials*, 2019. 216: 314–324.

49. Kabay, N., M. M. Tufekci, A. B. Kizilkanat, and D. Oktay. Properties of Concrete with Pumice Powder and Fly Ash as Cement Replacement Materials. *Construction and Building Materials*, 2015. 85: 1–8.

50. Hossain, K. M. A. Blended Cement Using Volcanic Ash and Pumice. *Cement and Concrete Research*, 2003. 33(10): 1601–1605.

51. Ramasamy, U., A. C. Bordelon, and P. J. Tikalsky. Properties of Different Pumice Grades Blended with Cement. *Journal of Materials in Civil Engineering ASCE*, 2017. 29(7).

52. Liu, J., X. J. Lv, M. L. Cao, and S. C. Cui. Experimental Study on Cementitious Property of Pumice. *Applied Mechanics and Materials*, 2011. 99–100: 773–776.

53. Tangtermsirikul, S., and P. Kitticharoenkiat. Development of Low Heat Concrete Using Fly Ash and Pumicite. *Research and Development Journal of the Engineering Institute of Thailand*, 1997. 1: 88–98.

54. Granata, M. F. Pumice Powder as Filler of Self-Compacting Concrete. *Construction and Building Materials*, 2015. 96: 581–590.

55. Öz, H. Ö., H. E. Yücel, and M. Günes. Freeze-Thaw Resistance of Self Compacting Concrete Incorporating Basic Pumice. *International Journal of Theoretical and Applied Mechanics*, 2016. 1: 285–291.

56. Li, Z. Drying Shrinkage Prediction of Paste Containing Meta-Kaolin and Ultrafine Fly Ash for Developing Ultra-High Performance Concrete. *Materials Today Communications*, 2016. 6: 74–80.

57. Tongbo, S., W. Bin, Z. Lijun, and C. Zhifeng. Meta-Kaolin for High Performance Concrete. In: Scrivener, K., Favier, A. (eds), Calcined Clays for Sustainable Concrete. *RILEM Bookseries*, 2015. 10: pp. 467–468.

58. Tafraoui, A., G. Escadeillas, S. Lebaili, and T. Vidal. Metakaolin in the Formulation of UHPC. *Construction and Building Materials*, 2009. 23(2): 669–674.

59. Mo, Z., R. Wang, and X. Gao. Hydration and Mechanical Properties of UHPC Matrix Containing Limestone and Different Levels of Metakaolin. *Construction and Building Materials*, 2020. 256: 119454.

60. Tafraoui, A., G. Escadeillas, and T. Vida. Durability of the Ultra High Performances Concrete Containing Metakaolin. *Construction and Building Materials*, 2016. 112: 980–987.

61. Song, Q., R. Yu, Z. Shui, Y. Wang, S. Rao, S. Wu, and Y. He. Physical and Chemical Coupling Effect of Metakaolin Induced Chloride Trapping Capacity Variation for Ultra High Performance Fibre Reinforced Concrete (UHPFRC). *Construction and Building Materials*, 2019. 223(7): 765–774.

62. Rangaraju, P. R., and Z. Li. Development of UHPC Using Ternary Blends of Ultra-Fine Class F Fly Ash, Meta-kaolin and Portland Cement. *International Interactive Symposium on Ultra-High Performance Concrete*, 2016. 1(1).

63. Gruber, K. A., T. Ramlochan, A. Boddy, R. Hooton, and M. Thomas. Increasing Concrete Durability with High-Reactivity Metakaolin. *Cement and Concrete Composites*, 2001. 23: 479–484.

64. Yazıcı, H., H. Yig˘iter, A.S. Karabulut, and B. Baradan. Utilization of Fly Ash and Ground Granulated Blast Furnace Slag as an Alternative Silica Source in Reactive Powder Concrete. *Fuel*, 2008. 87(12): 2401–2407.

65. Soutsos, M. N., S. J. Barnett, J. H. Bungey, and S. G. Millard. Fast Track Construction with High-Strength Concrete Mixes Containing Ground Granulated Blast Furnace Slag. *ACI SP*, 2005. 228–19: 255–270.

66. Shi, C., D. Wang, L. Wu, and Z. Wu. The Hydration and Microstructure of Ultra High Strength Concrete with Cement–Silica Fume–Slag Binder. *Cement and Concrete Composites*, 2015. 61: 44–52.

67. Tazawa E., and S. Miyazawa. Influence of Cement and Admixture on Autogenous Shrinkage of Cement Paste. *Cement and Concrete research*, 1995. 25: 281–287.

68. Lim, J. L. G., S. N. Raman, M. Safiuddin, M. F. M. Zain, and R. Hamid. Autogenous Shrinkage, Microstructure, and Strength of Ultra-High Performance Concrete Incorporating Carbon Nanofibers. *Materials*, 2019. 12(2): 320.

69. Kim, H., T. Koh, and S. Pyo. Enhancing Flowability and Sustainability of Ultra High Performance Concrete Incorporating High Replacement Levels of Industrial Slags. *Construction and Building Materials*, 2016. 123: 153–160.

70. Yalçınkaya, C., and H. Yazıcı. Effects of Ambient Temperature and Relative Humidity on Early-Age Shrinkage of UHPC with High-Volume Mineral Admixtures. *Construction and Building Materials*, 2017. 144: 252–259.

71. Ghafari, E., S. A. Ghahari, H. Costa, E. Júlio, A. Portugal, and L. Durães. Effect of Supplementary Cementitious Materials on Autogenous Shrinkage of Ultra-High Performance Concrete. *Construction and Building Materials*, 2016. 127: 43–48.

72. Tanesi, J. and R. Meininger. *Freeze-Thaw Resistance of Concrete with Marginal Air Content*. Publication No. FHWA-HRT-06-117. FHWA, U.S. Department of Transportation, 2006.

73. Papayianni, I., F. Kesikidou, and P. H. Alt. The Role of Shrinkage Reducing Admixtures and Supplementary Cementitious Materials in Volume Stability and Strength Development. *MATEC Web of Conferences*, 2019. 289.

74. Kristiawan, S., and M. T. M., Aditya. Effect of High-Volume Fly Ash on Shrinkage of Self-compacting Concrete. *Procedia Engineering*, 2015. 125: 705–712.

75. Portland Cement Association (PCA). Freeze-Thaw Resistance. https://www.cement.org/Learn/concrete-technology/durability/freeze-thaw-resistance. Accessed July 20, 2022.

76. Reiterman, P., O. Holčapek, O. Zobal, and M. Keppert. Freeze-Thaw Resistance of Cement Screed with Various Supplementary Cementitious Materials. *Reviews on Advanced Materials Science*, 2019. 58(1): 66–74.

77. Hill, R. L., and K. L. Folliard. The Impact of Fly Ash on Air-Entrained Concrete. *Concrete, tech talk,* 2006. pp. 71-72.

78. Joshi, P., and C. Chan. Rapid Chloride Permeability Testing. Hanley-Wood, LLC. 2002. Publication #C02L037.

79. Stanish, K. D., R. D. Hooton, and M. D. A. Thomas. *Testing the Chloride Penetration Resistance of Concrete: A Literature Review*. Contract No. DTFH61-97-R-000228. FHWA, U.S. Department of Transportation, 1997.

80. ASTM C157/C157M-17: *Standard Test Method for Length Change of Hardened Hydraulic-Cement Mortar and Concrete*. Annual Book of ASTM Standards. ASTM International, West Conshohocken, PA, 2017.

81. ASTM C666/C666M-15: *Standard Test Method for Resistance of Concrete to Rapid Freezing and Thawing*. Annual Book of ASTM Standards. ASTM International, West Conshohocken, PA, 2015.

82. ASTM C215-19: Standard Test Method for Fundamental Transverse, Longitudinal, and Torsional Resonant Frequencies of Concrete Specimens. Annual Book of ASTM Standards. ASTM International, West Conshohocken, PA, 2019.

83. ASTM C1202-22e1: Standard Test Method for Electrical Indication of Concrete's Ability to Resist Chloride Ion Penetration. Annual Book of ASTM Standards. ASTM International, West Conshohocken, PA, 2022.

84. AASHTO T 358: Standard Method of Test for Surface Resistivity Indication of Concrete's Ability to Resist Chloride Ion Penetration. Washington, D.C., 2019.

85. Toledo, W. K. and C. M. Newtson. Effects of Substrate Texture and Moisture Conditions on Ultra-High Performance Concrete and Silica Fume Concrete Overlay Bond Strengths. In Proceeding, 6th World Multidisciplinary Civil Engineering–Architecture-Urban Planning Symposium (WMCAUS), Prague. *IOP Conference Series: Materials Science and Engineering*, 2021. 1203: 032105.

86. ASTM C511-19: Standard Specification for Mixing Rooms, Moist Cabinets, Moist Rooms, and Water Storage Tanks Used in the Testing of Hydraulic Cements and Concretes. Annual Book of ASTM Standards ASTM International, West Conshohocken, PA, 2019.

87. ASTM C143/C143M-20: *Standard Test Method for Slump of Hydraulic-Cement Concrete. Annual Book of ASTM Standards*. Annual Book of ASTM Standards. ASTM International, West Conshohocken, PA, 2020.

88. ASTM C1611/C1611M-21: *Standard Test Method for Slump Flow of Self-Consolidating Concrete*. Annual Book of ASTM Standards. ASTM International, West Conshohocken, PA, 2021.

89. BS1881: *Method for Determination of Compressive Strength of Concrete Cubes*. British Standard Testing concrete Part 116, London, UK, 1983.

90. ASTM C1609/C1609M-19a: Standard Test Method for Flexural Performance of Fiber-Reinforced Concrete (Using Beam with Third-Point Loading). Annual Book of ASTM Standards. ASTM International, West Conshohocken, PA, 2019.

91. Newtson, C., B. Weldon, J. Garcia, S. Mousavinezhad, and W. Toledo. Durability of Concrete Produced with Alternative Supplementary Cementitious Material. *Final Research Report*, Tran-SET project 20CNMSU40, Transportation Consortium of South-Central States, Louisiana State University, 2021. Retrieved from https://digitalcommons.lsu.edu/transet_pubs/109.

92. Tanesi, J., B. Graybeal, and M. Simon. Effects of Curing Procedure on Freeze-Thaw Durability of Ultra-High Performance Concrete. *6th International RILEM Symposium on Fibre Reinforced Concretes*, Varenna, Italy, 2004. 1: 603–613.

93. Parande, A. K., B. R. Babu, M. A. Karthik, K. K. Deepak Kumaar, and N. Palaniswamy. Study on Strength and Corrosion Performance for Steel Embedded in Metakaolin Blended Concrete/Mortar. *Construction and Building Materials*, 2008. 22(3): 127–134.

94. Streicher, P. E., and M. G. Alexander. A Chloride Conduction Test for Concrete. *Cement and Concrete Research*, 1995. 25(6): 1284–1294.